Unlocking the potential of 2D nanomaterials for sustainable intelligent packaging

Chemical Engineering Journal 490 (2024) 151711

Contents lists available at ScienceDirect

Chemical Engineering Journal

journal homepage: www.elsevier.com/locate/cej

Unlocking the potential of 2D nanomaterials for sustainable intelligent packaging

Shima Jafarzadeh [a,*], Majid Nooshkam [b], Zeinab Qazanfarzadeh [c], Nazila Oladzadabbasabadi [d], Przemyslaw Strachowski [e], Navid Rabiee [f,g], Kamyar Shirvanimoghaddam [h], Mehdi Abdollahi [i], Minoo Naebe [h,*]

[a] Centre for Sustainable Bioproducts, Deakin University, Waurn Ponds, VIC 3216, Australia
[b] Department of Food Science and Technology, Faculty of Agriculture, Ferdowsi University of Mashhad (FUM), Mashhad, Iran
[c] International Centre for Research on Innovative Biobased Materials (ICRI-BioM)-International Research Agenda, Lodz University of Technology, Żeromskiego 116, 90-924 Lodz, Poland
[d] School of Science, STEM College, RMIT University, Melbourne, VIC 3001, Australia
[e] Department of Biology and Biological Engineering-Food and Nutrition Science, Chalmers University of Technology, SE 412 96 Gothenburg, Sweden
[f] School of Engineering, Macquarie University, Sydney, New South Wales, 2109, Australia
[g] Centre for Molecular Medicine and Innovative Therapeutics, Murdoch University, Perth, WA 6150, Australia
[h] Institute for Frontier Materials, Deakin University, Waurn Ponds, Geelong, Victoria 3216, Australia
[i] Department of Life Sciences, Chalmers University of Technology, SE 412 96 Gothenburg, Sweden

ARTICLE INFO

Keywords:
Intelligent packaging
Two-dimensional nanomaterials
Nanocomposite
Food packaging
Shelf life

ABSTRACT

The demand for high food safety standards, spoilage prevention, and the minimization of food waste has spurred extensive investigation into intelligent food packaging. Within this field, considerable attention has been directed towards two-dimensional (2D) nanomaterials owing to their exceptionally thin layered configuration and diverse physicochemical, electrical, optical, and thermal properties. These attributes render 2D nanomaterials highly suitable for enhancing sensing capabilities in intelligent packaging systems. This review delves into the forefront of research concerning the utilization of 2D nanomaterials in intelligent packaging applications. It provides a comprehensive survey of intelligent food packaging concepts and explores various 2D materials, including graphene-based materials, MXene, and silicate clay, investigated for their potential in intelligent packaging systems. Additionally, the review interprets the structure, properties, and utilization of 2D materials in diverse biosensing systems encompassing gas, moisture, pH, and bacteria sensors, indicators, or wireless tags. Moreover, it examines the influence of 2D materials on the mechanical, optical, thermal, barrier, and bioactive properties of smart packaging, while also deliberating on their respective advantages and limitations. By combining these foundational elements, this study offers a distinctive and thorough contribution to the domain of food packaging, laying the groundwork for the future development of sustainable and high-performance packaging materials.

1. Introduction

Packaging, storage conditions, and transportation factors significantly influence food quality and shelf life [1,2]. As such, it is difficult to accurately estimate the food expiry date, resulting in food spoiling before its printed expiration date and causing food poisoning [3,4]. The World Health Organization (WHO) reported in 2017 that spoiled foods cause 600 million illnesses and 420,000 deaths annually [5]. On the other hand, the printed expiration date and best-before date frequently are inaccurate at predicting food shelf-life, resulting in unnecessary disposal of non-spoiled food items. Foodbank highlights that approximately 70 % of discarded food remains perfectly edible, contributing to a global problem where roughly one-third of all produced food never reaches human consumption, leading to excessive waste and foodborne diseases [6]. These issues primarily arise from the lack of real-time quality and freshness monitoring, coupled with the rapid growth of microorganisms and metabolite changes. However, a promising solution to prevent spoilage and reduce waste can be found in smart packaging. Smart packaging, which integrates intelligent and active systems, addresses the underlying causes of food spoilage and waste [7]. Intelligent

* Corresponding authors.
E-mail addresses: s.jafarzadeh@deakin.edu.au (S. Jafarzadeh), minoo.naebe@deakin.edu.au (M. Naebe).

https://doi.org/10.1016/j.cej.2024.151711

Available online 26 April 2024

packaging provides real-time data on food quality and introduces dynamic expiration dates through innovative indicators and sensors. This transition from static shelf life to dynamic shelf life reduces food waste and protects consumers against potential foodborne illnesses [8,9].

The emergence of nanotechnology has opened up new possibilities for the development of advanced intelligent packaging [10,11]. Within the diverse category of nanomaterials, two-dimensional materials (2D) have emerged as a novel and promising class with considerable potential in the field of food packaging [12]. A 2D material is defined as a material where the atomic arrangement and bond strength are notably stronger across two dimensions than in a third dimension [13]. These materials are distinguished by their layered structures and exhibit exceptional characteristics of having a single or only a few atoms in thickness, often measuring less than 5 nm [14]. Interestingly, their lateral dimensions can extend beyond 100 nm, and in some cases, even reach a few micrometers [15]. Their high surface-to-volume ratio, which is different from bulk materials, is their most important property. This property is advantageous for the transport of mass and heat, as well as for ion diffusion [16]. Graphen and its derivatives, (i.e. graphene oxide (GO) and reduced graphene oxide (rGO)), MXenes, and silicate clay are the most used 2D materials in intelligent food packaging systems.

The structural composition of 2D materials exhibits heightened physicochemical, optical, and electronic attributes, primarily influenced by distinctive characteristics such as phase their size, stability, crystallinity, and exfoliation level. These attributes may vary based on the synthesis approach utilized. Recently, these specific attributes of 2D materials have been found to significantly enhance the performance metrics of sensing and biosensing systems, particularly in optical and electrochemical transduction approaches [16,17]. This renders them promising candidates for intelligent food packaging, enabling the detection of various analytes and changes created during food shelf-life. A 2D material can be tailored to act as a sensor, colorimetric indicator, or wireless tag to detect temperature changes, gas concentrations, and specific substances present within the packaging. In this manner, the packaged food is monitored in real-time to ensure its quality and safety. Moreover, they can be designed to react to specific triggers, such as pH change, temperature change, moisture or gas composition change, making them highly customizable [18,19]. Furthermore, 2D materials possess the potential to offer packaging materials with bioactive properties such as antioxidant and antibacterial activities, while also impacting package characteristics such as mechanical strength, barrier properties, optical clarity, and thermal conductivity.

Despite the exceptional properties of 2D materials and widely available research on their application in intelligent food packaging and providing excellent functions, to the best of our knowledge, there has been no comprehensive review to date on the potential effects of 2D materials on intelligent food packaging. This review article provides an overview of various 2D nanomaterials and their structures and properties. Additionally, 2D nanomaterials are explored in various intelligent packaging applications including sensors, colorimetric indicators, and wireless tags. We also examine how 2D nanomaterials affect smart packaging properties such as barrier, thermal, mechanical, and antimicrobial properties. Lastly, it discusses the pros and cons of 2D nanomaterials in intelligent packaging. The general overview of the present review is shown in Fig. 1.

2. Intelligent food packaging

Conventional plastic packaging limitations, which often are unable to accurately display real-time food expiration dates, contribute to both food waste and the risk of foodborne diseases. Food products' quality and shelf life are significantly influenced by factors such as packaging, storage conditions, and transportation. Consequently, it becomes challenging to accurately determine the true expiry date of food items, resulting in food spoilage before the printed expiration date and the potential risk of foodborne illnesses [8]. According to a 2017 report by

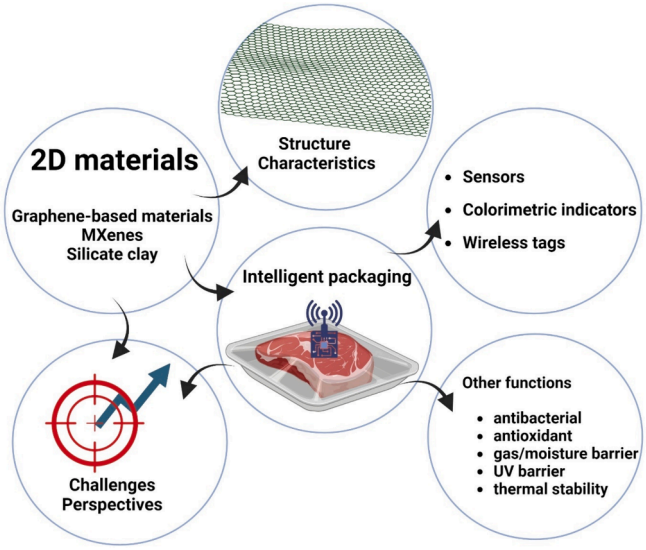

Fig. 1. Schematic overview of the present review.

the World Health Organization (WHO), spoiled foods lead to approximately 600 million cases of illness and 420,000 deaths annually [5]. In contrast, the printed expiration date and best-before date may not consistently align with the actual shelf life of a product, leading consumers to discard items that are still safe to consume. Intelligent packaging, incorporating both intelligent and active systems, offers solutions to these issues by providing real-time information on food quality and dynamic expiration dates using indicators and sensors. This transition from fixed to dynamic shelf life reduces food waste and protects consumers against foodborne illnesses [20]. Some smart packaging solutions, containing active agents, enhance food shelf life and quality by controlling oxygen levels, inhibiting microbial growth, and preventing unwanted metabolic changes [21,22]. Intelligent packaging includes smart sensors, time–temperature indicators, and smart labels, each serving a specific purpose [3]. Overall, as technology advances and sustainability and food safety become more important, intelligent food packaging continues to develop. Consumers will be able to enjoy both convenience and safety by using this type of packaging, while environmental concerns are also addressed.

3. 2D nanomaterials: Structures, Properties, and synthesis

Among the diverse categories of nanomaterials, 2D nanomaterials have emerged as a promising class with significant potential. Diverse 2D nanomaterials, including graphene, GO, rGO, MXenes, and layered silicate have shown considerable potential in intelligent packaging. The molecular structure of these materials is shown in Fig. 2. Ultrathin 2D materials possess a diverse set of unique properties that make them exceptional materials within the field of nanomaterials. These nanomaterials, characterized by their high diameter-to-length ratio, exhibit especially unique properties compared to their bulkier counterparts. While certain properties can broadly be generalized, it's critical to note that not all ultrathin 2D nanomaterials will necessarily exhibit these unique properties. High surface area is a defining characteristic possessed by all types of 2D nanomaterials [23]. The remarkable flexibility of 2D nanomaterials represents a highly valuable attribute, particularly in the development of flexible electronics and sensors. Unlike traditional semiconductor and metal-based strain sensors, which tend to be brittle and rigid, 2D nanomaterials' high flexibility makes them an excellent choice for designing flexible sensors for intelligent packaging [24]. Furthermore, 2D nanomaterials exhibit extraordinary optical properties, fuelling extensive exploration in this field. These unique optical characteristics become especially prominent when

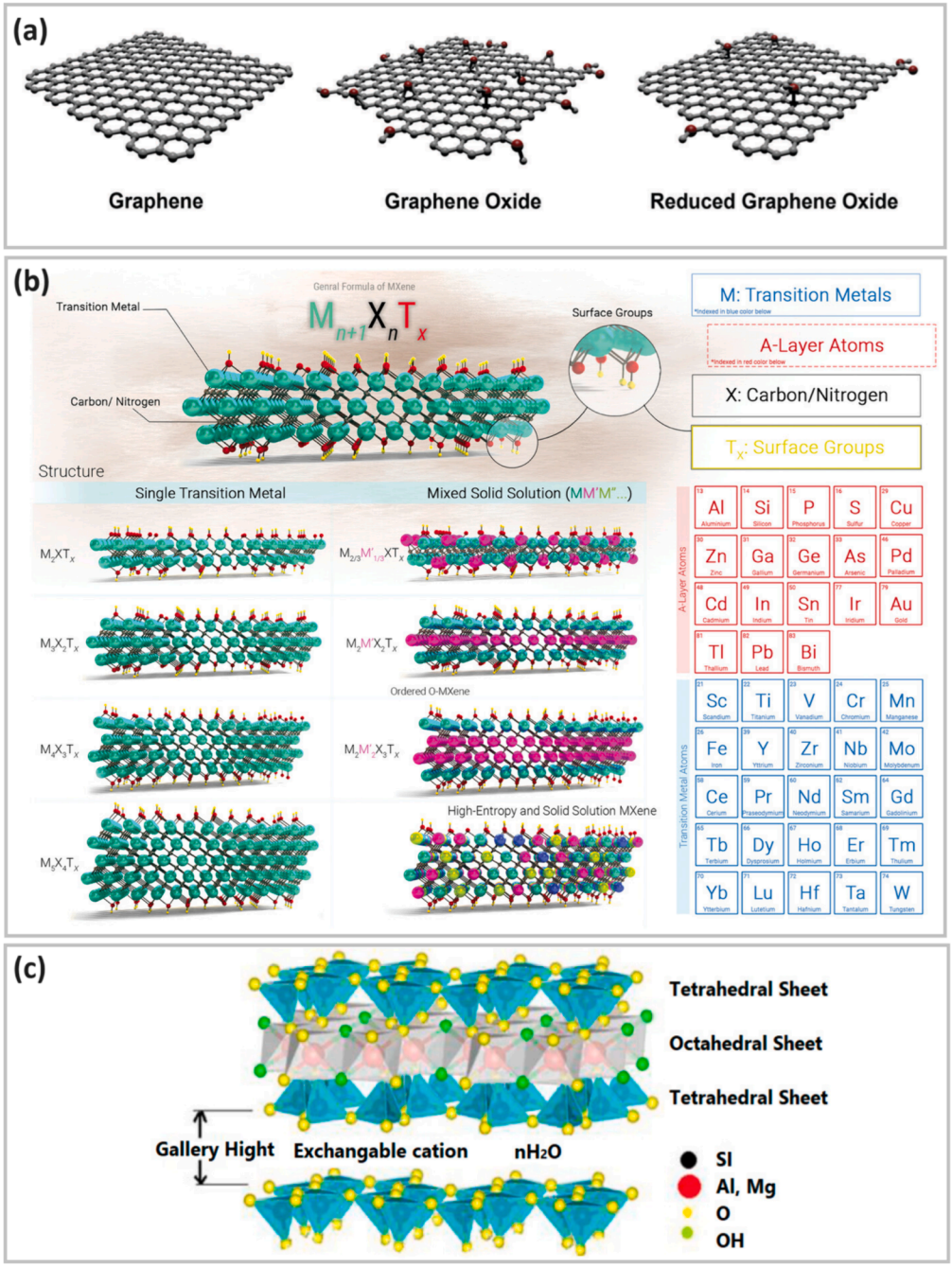

Fig. 2. (a) Different molecular structures of graphene-based materials useful for intelligent packaging. Reprinted with permission from [26]. (b)Various structural forms of MXenes and potential elements have been employed in the production of diverse MAX phases. Reprinted (reproduced) with permission from [27], John Wiley & Sons. (c) Structure of 2:1 layered silicate. Reprinted with permission from [28].

ultrathin 2D nanomaterials are reduced to a single or a few atomic layers. Such distinctive optical attributes include plasmonic effects, light sensitivity, emission, and absorption. Their susceptibility to external environmental factors, coupled with their optical capabilities, has generated notable interest in optical sensor advancement [25].

In addition to their optical capabilities, 2D nanomaterials have exceptional mechanical strength and can tolerate high stress. For many 2D nanomaterials, Young's modulus typically falls within the range of 150 to 400 GPa. Given these outstanding properties, 2D nanomaterials are an excellent choice for enhancing composite properties when used as nanofillers. Consequently, these extraordinary attributes have made 2D ultrathin materials at the forefront of research in various fields, including separations, sensors, membrane fabrication, and intelligent food packaging.

3.1. Carbon-based 2D materials

Carbon-based materials have garnered a lot of interest in the field of 2D materials since the discovery of graphene. These materials have a wide range of applications, including catalysis, adsorption, and electrical energy storage. The porous structure of these carbon-based materials plays a crucial role in determining their properties [16]. Carbon-based 2D materials, such as graphene and its derivatives (i.e., GO and rGO), have attracted significant attention for their potential applications in intelligent food packaging.

3.1.1. Graphene

The isolation of graphene from graphite in 2004 marked the beginning of the real exploration of 2D nanomaterials and a significant milestone in materials chemistry. It reinforced the theory that materials when engineered into single or few-atom-thick layers can exhibit exceptional performance across various applications. Consequently, the investigation of 2D nanomaterials commenced, leading to the introduction of several new 2D materials, both through experimentation and theoretical exploration [29].

Due to its remarkable properties, graphene has been studied extensively since its discovery [30–33]. These include an up to 2600 m^2/g theoretical surface area, 4840–5300 W m^{-1} K^{-1} thermal conductivity, up to 130 GPa tensile strength, 1000 GPa elastic modulus, and 200,000 cm^2 V^{-1} s^{-1} electron mobilities. It is made up of hexagonally arranged carbon atoms that are arranged in a plane that is one atom thick, where the carbon atoms are sp^2 hybridized and bonded together [34] (Fig. 2**a**). Graphene is effective in the field of intelligent food packaging, where it enhances its barrier, thermal, and mechanical attributes. Moreover, like

Table 1
Summary of research involving the synthesis of graphene and graphene derivatives from diverse carbon-based .

Source	Method and conditions	Graphene type	Remarks	References
Gases				
Methane (CH_4)	Graphene was produced on a copper foil using plasma-enhanced CVD, without the presence of an H_2 flow.	Single layer graphene	High quality graphene	[43]
	Graphene was produced in a continuous manner in the gas phase through a one-step pyrolysis process using methane. This was accomplished using an alternative-current arc plasma, under atmospheric conditions and without the need for a substrate.	Few layer graphene	High purity graphene with the yield of more than 2 g/h	[44]
	Methane was decomposed on MgO above 778 °C during CVD process.	Graphene mesosponge (consisting mainly of single layer graphene walls)	The graphene mesosponge derived from MgO possesses a unique set of characteristics, including a large surface area, well-developed mesopores, and high resistance to oxidation. Additionally, it exhibits significant softness and elasticity, a very low bulk modulus of 0.05 GPa, and the ability to undergo a reversible liquid–gas phase transition when subjected to force.	[45]
	A group of Fe-Mo-Mg catalysts were tested for their effectiveness in synthesizing hybrid materials composed of graphene nanosheets and carbon nanotubes. This was accomplished through the use of methane CVD.	Graphene nanosheets	High quality graphene nanosheets	[46]
CO	Al_2S_3 was calcined under a mixed gas flow of CO and Ar.	Few layer graphene sheets	The sheets were transparent	[47]
CO_2	Burning magnesium metal in dry ice	Few layer graphene nanosheets	High yield graphene	[48]
	CVD; copper foils; 1060 °C	Few layer graphene	This approach allows for the production of graphene films without the use of elemental hydrogen. The resulting graphene layers are of higher quality compared to those produced using conventional CVD processes that rely on a combination of hydrogen and methane.	[49]
Liquids				
Methanol, ethanol, propanol	CVD; copper foils; 850 °C; 5 min	Single layer graphene	High quality graphene	[50]
Benzene	CVD; copper foils; > 825 °C; 30 min	Single layer graphene	High quality graphene	[51]
Hexane	CVD; copper foils; 1000 °C; 15 min	Few layer graphene	The approximate number of layers was calculated to be 11.	[52]
Toluene	Graphene flakes were produced through the process of micromechanical cleavage of natural graphite. These flakes were then positioned on a silicon substrate that had been heavily doped and coated with a layer of silica that was 300 nm thick.	Single layer graphene	In the presence of graphene, toluene was observed to function as an electron donor, transferring electrons to the graphene.	[53]
Solids				
Camphor	Layers of graphene were deposited onto a copper foil using a microwave surface-wave plasma CVD process. This was accomplished at a relatively low temperature, below 600 °C.	Few layer graphene	Fully flexible transparent electrode was fabricated by the graphene film.	[54]
Alfalfa shoots	The dried alfalfa shoots were shaken in 2.5 M HNO_3 at 70 °C for 300 min.	Graphene sheets	The final product was found to be pure and well-graphitized.	[55]
Rice husk	Graphene nanosheets were produced through a process that involved the carbonization of brown-rice husks. This was followed by a one-stage activation process using potassium hydroxide (KOH).	Ultrathin graphene nanosheets	A sustainable electrochemical energy-storage electrode was developed by the graphene nanosheets.	[56]
Tea waste biomass	The tea waste was first dried and then carbonized at a temperature of 650 °C in an argon atmosphere. The resulting carbonized sample was then oxidized to synthesize graphene oxide (GO). To produce reduced graphene oxide (rGO), the sample was heated at 250 °C for 30 min in an argon gas atmosphere.	GO and rGO	The graphene oxide (GO) that was obtained has shown great potential for the degradation of various pollutants in water.	[57]
Cane molasses	Graphene was synthesized by introducing pure graphite into a solution of molasses and subjecting it to sonication via a probe, while gently stirring at room temperature for a duration of 3 h.	Few layer graphene	The graphene synthesis was green, simple, easily scalable, fast, and highly efficient.	[58]

Sources

several other 2D materials, graphene exhibits potent antibacterial properties due to its capacity to interact with cell membranes and absorb phospholipids [35–37]. Consequently, certain polymer-graphene nanocomposites demonstrate strong antibacterial activities. Additionally, graphene finds applications in producing preservative emitters and innovative devices for intelligent packaging, capitalizing on its high surface area and excellent electrocatalytic capabilities [38]. In this regard, graphene has also been used to develop sensors that can detect food spoilage. These sensors can monitor changes in pH, temperature, and gas composition within the food package, providing an early warning system for spoilage before it becomes visible [39].

Graphene can be synthesized from various carbon-based sources, including gases, liquids, and solids (Table 1). The most common process for creating graphene is chemical vapor deposition (CVD) because it can continuously deposit a high-quality graphene film over various transition metals that are used as catalysts. The hydrocarbon source is decomposed on the metal surface during the CVD process to create the layers of graphene. There are two distinct graphene growth mechanisms: surface and segregation ones, depending on the transition metals used. Graphene layers begin to form on the surface of metals with low carbon solubility as soon as the hydrocarbon source decomposes. The growth of these layers ceases when the flow of the hydrocarbon source is stopped. For metals that have a high solubility for carbon, the segregation growth mechanism is observed. This process begins when the concentration of carbon atoms in the bulk metal reaches a certain level, and nucleation takes place while cooling. When there is an excess of diluted carbon atoms, they move towards the metal surface. This causes the carbon atoms to segregate and form graphene. This process continues until the carbon concentration in the metal decreases to an equilibrium level. This happens even if the supply of hydrocarbons has been stopped, unlike the surface growth mechanism [40,41].

Methane (CH_4) stands as one of the extensively utilized gaseous precursors in the development of graphene films and is a prevalent source of carbon in the CVD process. Moreover, gases that encompass carbon, such as CO and CO_2, have been employed in the fabrication of graphene (Table 1). Nickel (Ni) and Copper (Cu) are commonly chosen catalysts for graphene synthesis due to their substantial grain size, cost-effectiveness, and etching capabilities. The ability of carbon to dissolve easily allows both single-crystalline Ni(1 1 1) and polycrystalline Ni to produce graphene. Large graphene films are also produced using readily available polycrystalline Ni foil. Although the thicknesses and number of layers of the graphene made from polycrystalline Ni are always found to vary (Fig. 3). Lattice steps are abundant in polycrystalline Ni, which has a lot of grain boundaries. These lattice steps are where the majority of multilayer graphene is created. This is as a result of the grain edge's curvature, which enables carbon to gather in these places and results in the nucleation of multilayer graphene, as depicted in Fig. 3**b**. On the other hand, the smooth surface of single-crystal Ni(1 1 1) promotes the nucleation of monolayer graphene, as shown in Fig. 3**a** [42]. Due to polycrystalline Ni's high carbon solubility, multilayer graphene always forms on this material.

The mechanism of graphene nucleation and extension catalyzed by Cu is different from other transition metals. It has been proposed that a chemisorption/deposition or surface growth approach is used. Since carbon does not dissolve very well in the bulk of copper, it can be inferred that the process of carbon mobility is entirely surface-based. Cu also has a lower barrier to carbon atom diffusion than other transition metals, which gives it a unique catalytic function [41].

The synthesis of graphene has also been achieved through the use of liquid precursors such as benzene, toluene, xylene, hexane, ethanol, methanol, propanol, and different natural carbon-bearing precursors (Table 1) [34,53,59]. For instance, researchers reported layer-by-layer CVD growth of graphene on templates made of mechanically exfoliated graphite crystals [60]. They used a custom-built CVD apparatus

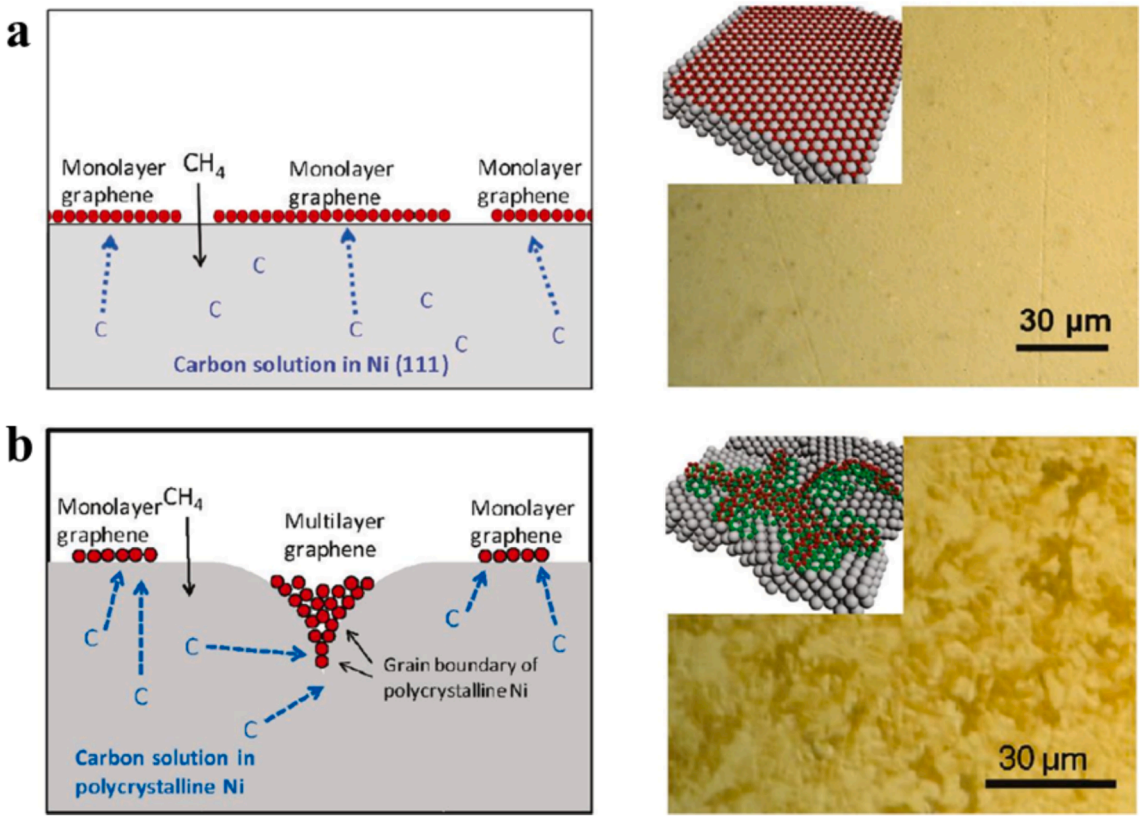

Fig. 3. The diagrams illustrate the mechanism of graphene growth on (a) Ni (1 1 1) and (b) polycrystalline Ni surfaces, along with the corresponding optical images of graphene/Ni (1 1 1) and graphene/polycrystalline Ni surfaces after the CVD process. Reprinted with permission from [58].

with three independently controlled temperature zones and ethanol as the carbon feedstock. The authors claim that employing multiple temperature zones in CVD processing may offer greater control and wider temperature windows, making it better suited for graphene layer growth. In this context, the ethanol thermal decomposition and the growth of graphene typically occur at temperature ranges of 870–900 °C and 680–740 °C, respectively. The authors have presented a diagram that illustrates their proposed theory on how graphene grows on graphene templates (Fig. 4). Their hypothesis states that the carbon species created by the thermal breakdown of ethanol fall onto the graphene flakes and spread out over the surface (Fig. 4**a**). On the surface of pre-existing graphene flakes, new graphene nuclei are formed, as shown in Fig. 4**b**. It is clear from the shape and size of the graphene flakes formed after CVD that the edge sites of the original graphene flakes are not active for graphene growth. The graphene nuclei undergo rapid lateral expansion, resulting in the formation of a new layer of graphene, as depicted in Fig. 4**c**. The growth of graphene on the sides must happen much faster than the formation of new graphene nuclei. This is because even layers of graphene were observed on the terraces without multiple nucleation formation. This means that the formation of new particles (nuclei) is what controls the speed of the graphene growth. As new terraces are created, more graphene nuclei form, and the growth continues layer by layer (Fig. 4**d**).

A variety of solid materials can be used to create graphene by decomposing at high temperatures (as shown in Table 1). Ruan et al. (2011) used a variety of materials, including food, insects, and waste, as the carbon source to create monolayer graphene [61]. Some of the materials they used included cookies, chocolate, grass, plastic, dog feces, and roaches. By heating these materials to 1050 °C in a hydrogen/argon flow on a copper foil, they were able to produce a high-quality graphene film (Fig. 5**A, B**). The Raman spectrum of these films did not show significant disorder (D) bands, indicating that there were very few defects present. Additionally, the large ratio of the 2D band to the G band suggested that the graphene produced was a monolayer film [61]. Since the CVD growth of high-quality graphene requires a nearly oxygen-free environment or high-vacuum base pressure, a long pumping and/or purge time is needed to evacuate the air in the chamber [62]. In addition to the CVD techniques, graphene can be synthesized with various techniques which can be greener and much simpler. Pyrolysis coupling with hydrothermal carbonization pretreatment was utilized to synthesize graphene from fungus. The dried fungus (*Auricularia*) underwent hydrothermal pretreatment in KOH (120 ℃, 6 h), followed by freeze drying and activation under N_2 in a tube furnace (800℃, 1 h) (Fig. 5**C**). This method led to densely porous graphene-like carbon materials with 10 nm in thickness [63]. As another green method, microwave plasma irradiation was employed for nanocarbon growth from rice husk. In this method, rice husk was placed on a homemade nickel case located on a stage. The nickel foil was irradiated to produce the nickel atoms, which tend to aggregate with each other by reducing surface energy, resulting in the formation of nickel clusters. The resulting nickel clusters with irregular shapes in the usual 30–150 nm size initiated and accelerated the graphitization process by assembling carbon radicals into graphene surrounding the nickel clusters. The nickel cases were covered by a soot-like appearance which included ball- and fibre-like materials. This technique generated carbon nanotubes and graphenated carbon nanotubes beside the graphene (Fig. 5**D**) [64]. It could be also noteworthy that a large amount of bio-waste from animal and agricultural sources is discarded into the environment annually. Despite being biodegradable and produced in large quantities, these wastes can be used as precursors for graphene production, adding value to their consumption and expanding their potential applications (Table 1).

3.1.2. *Graphene oxide (GO)*

Graphene oxide, or GO, is a material that is derived from graphene. It is created through a two-step process that involves the chemical oxidation of graphite using strong acids, which produces graphite oxide. The graphite oxide is then exfoliated into single layers through either stirring or mild sonication, which is a mechanical process [65,66]. GO is therefore a layer of carbon that contains several oxygen functional groups, including carboxylic, hydroxyl, and epoxy. These functional groups are located on the basal planes and edges of the GO layer. As a result, the structure of GO is a hybrid of sp^2 and sp^3 configurations [67]. The proposed structure of GO is depicted in Fig. 2**a**.

The high level of oxygen has been shown to be very beneficial for chemically altering or adding functionality to other molecules. This allows it to be dispersed in various matrices, resulting in the creation of nanocomposites with intriguing properties [68]. GO preserves numerous graphene properties, yet it offers the advantages of being more cost-effective and simpler to produce at scale. This ease of production and processing is attributed to its superior solubility in various solvents. The chemical exfoliation of graphite in an oxidative environment leads to stable aqueous suspensions of GO [36]. GO acts as an

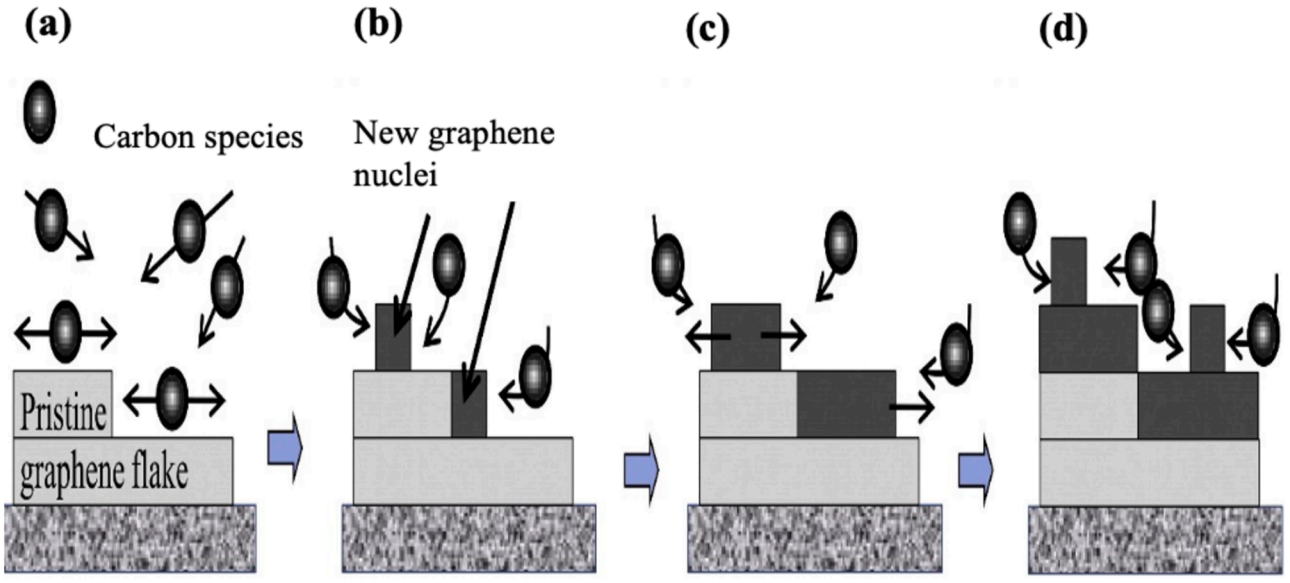

Fig. 4. A diagram that shows the step-by-step process of how graphene grows layer by layer using CVD with ethanol as the .
Source material. Reprinted with permission from [60]

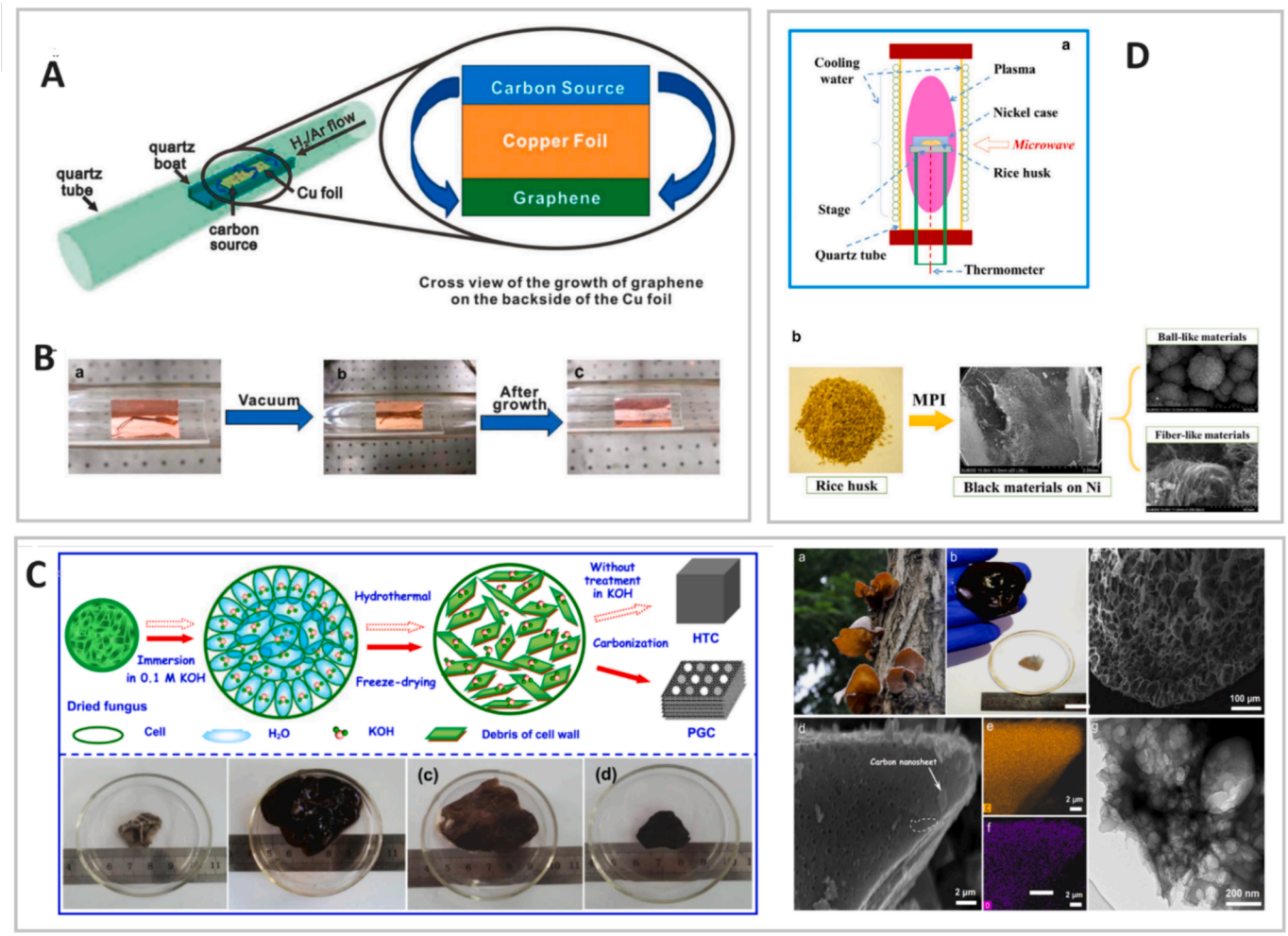

Fig. 5. Synthesis of graphene from different biomass . (C) Left: Schematic of hydrothermal treated carbon (HTC, untreated with KOH) alongside compact, densely porous graphene-like carbon (PGC) materials from fungus (Auricularia) biomass; Initial dried fungus state (a); fungus swollen post-hydrothermal treatment in 0.1 M KOH solution (b); freeze-dried fungus following hydrothermal treatment (c); carbon materials obtained through the carbonization of freeze-dried fungus (d). Right: Image depicting naturally abundant fungus (a), dried fungus in a Petri dish and fungus expanded after undergoing hydrothermal treatment (b), Scanning electron microscopy (SEM) image showcasing freeze-dried fungus following hydrothermal treatment in 0.1 M KOH (c), SEM image featuring the densely porous layer-stacked carbon (PGC) material (d), corresponding elemental mapping images of carbon and oxygen atoms (e, f), High resolution transmission electron microscopy (TEM) image of PGC, revealing an interconnected porous system (g). Reprinted with permission from . (D) Illustration depicting the microwave plasma irradiation technique for nanocarbon growth from rice husks (a), the transformation of rice husks into soot-like materials on the nickel surface, characterized by the presence of ball- and fiber-like structures during the conversion process (b). Reprinted with permission from .
Sources. (A) Schematic of the experimental setup designed for synthesizing graphene from various sources such as food, insects, or waste within a tube furnace. A copper foil containing the carbon source is placed within a quartz boat and situated within the high-temperature region of the tube furnace. The growth process is conducted at 1050°C under reduced pressure by a flow of H_2/Ar gas. The high-quality graphene is produced on the underside of the copper substrate. (B) Process of graphene synthesis utilizing a cockroach leg including placement of a single cockroach leg atop the copper foil (a), applying of vacuum conditions to the roach leg (b) and residue remaining after subjecting the roach leg to annealing at 1050°C for 15 min. Reprinted with permission from [61][63][64]

insulator because of the presence of defects and oxygen groups that separate the sp^2 regions. It has excellent photoluminescence properties, making it ideal for use in bio-sensing and photoelectronics. GO can also be applied in composites, drug/gene delivery, sorption materials, and energy storage. The thin films of GO can be easily produced by filtration or drop-casting, forming membranes that are highly permeable to water molecules but impermeable to other molecules and even atoms such as nitrogen and oxygen [66,69]. In GO membranes, water transportation is influenced by the interaction between oxygen groups and water molecules. The oxygen groups in the hydrophilic domains interact strongly with water molecules, impeding their momentum, while the hydrophobic sp^2 patches accelerate them [66].

GO nanoplatelets have garnered significant attention for humidity and gas sensing, as well as semiconductor photocatalyst material owing to their distinctive chemical composition and expansive specific surface areas. GO functionalized with folic acid was employed as a humidity sensor within the chitosan-polyvinyl alcohol (PVA) matrix. This functionalization an augmentation of the D-spacing distance within GO nanosheets (from 7.39 to 9.36 Å), indicating the infiltration of folic acid between their stacked layers. The sensing mechanism delineated the chemical interaction between water molecules and the sensor surface at a low moisture level. While at the higher moisture content, it revealed the generation of hydronium ions through the physisorption of the water molecule onto the chemisorption layer. The integration of reactive sites present in folic acid (COOH, NH_2, and NH) significantly enhanced the sensing efficacy of GO. Additionally, this incorporation bolstered the tensile strength of the sensor matrix (from 38 to 70 MPa) and introduced antibacterial properties against both gram-positive and gram-negative bacteria [70]. Furthermore, GO found application in enhancing the physio-mechanical and thermal attributes of intelligent packaging

systems. For instance, GO (synthesized from graphite with sulfuric and phosphoric acid) incorporated into a matrix comprising soybean polysaccharides and grape skin anthocyanin served as a colorimetric pH indicator for monitoring Salamon fish spoilage. Characterization of GO morphology revealed singular layers of nanosheets with specific thickness of 1.2–1.5 nm and lateral dimensions of less than 1 μm, along with notable transparency and flexibility (Fig. 6). Integration of GO into the packaging film mitigated weaknesses attributed to anthocyanins, while simultaneously enhancing mechanical and thermal properties, and reducing the water sensitivity of the indicator [71].

4.

4.0.1. Reduced GO (rGO)

For some practical uses of GO, such as when it needs to be incorporated into a hydrophobic polymeric matrix, a reduced form may be more appropriate. GO can be reduced to rGO through various methods including chemical, thermal, photo-chemical, photo-thermal, microwave, or microbial/bacterial. This reduction can partially or completely restore the hybridized sp^2 configuration of the material, bringing it closer to the graphene configuration (Fig. 2**a**) [36]. The rGO has properties similar to those of pristine graphene in terms of mechanics, optoelectronics, and conductivity. This is due to its heterogeneous structure, which consists of a graphene-like basal plane with additional structural defects and areas containing oxidized chemical groups. These graphene-like properties make rGO a highly sought-after material for use in a wide range of applications, including sensors, biology, the environment, catalysis, optoelectronics, and storage devices. The rGO not only has good absorption properties across the entire spectrum, with even a single layer capable of absorbing a significant amount of light in the visible and near-infrared range, but it also has functional groups that allow it to be dispersed in various solvents. However, it is important to note that rGO tends to clump together during the reduction process, so much research is focused on not only reducing but also stabilizing rGO using different methods [72]. In recent years, the development of nanotechnology has led to the frequent use of rGO nanocomposites in the construction of electrochemical biosensors. This is due to their unique physical and chemical properties, as well as their biocompatibility. Combining rGO nanocomposites with biomolecules that have specific recognition capabilities provides a promising approach for creating more stable and sensitive electrochemical biosensors for detecting different factors and foodborne pathogenic bacteria [73]. As an example of rGO application in intelligent packaging for sensing the pressure applied to a product during transportation or preservation, an rGO-based pressure sensor was developed. In this study, the rGO aerogel sensor was fabricated in combination with aramid nanofiber (ANF) and polyaniline nanotube (PANIT). GO was employed to synthesize the rGO during the aerogel preparation through thermal treatment and freeze-drying approaches. The composite gels were formed through the strong interactions between PANIT, rGO, and ANF. The final aerogel sensor showed good mechanical strength, compressibility, and high conductivity with high sensitivity (1.73 KPa^{-1}), low detection limit (40 Pa) in a short time as well as high compressive cycle stability (3000 cycles) [74] (Fig. 7).

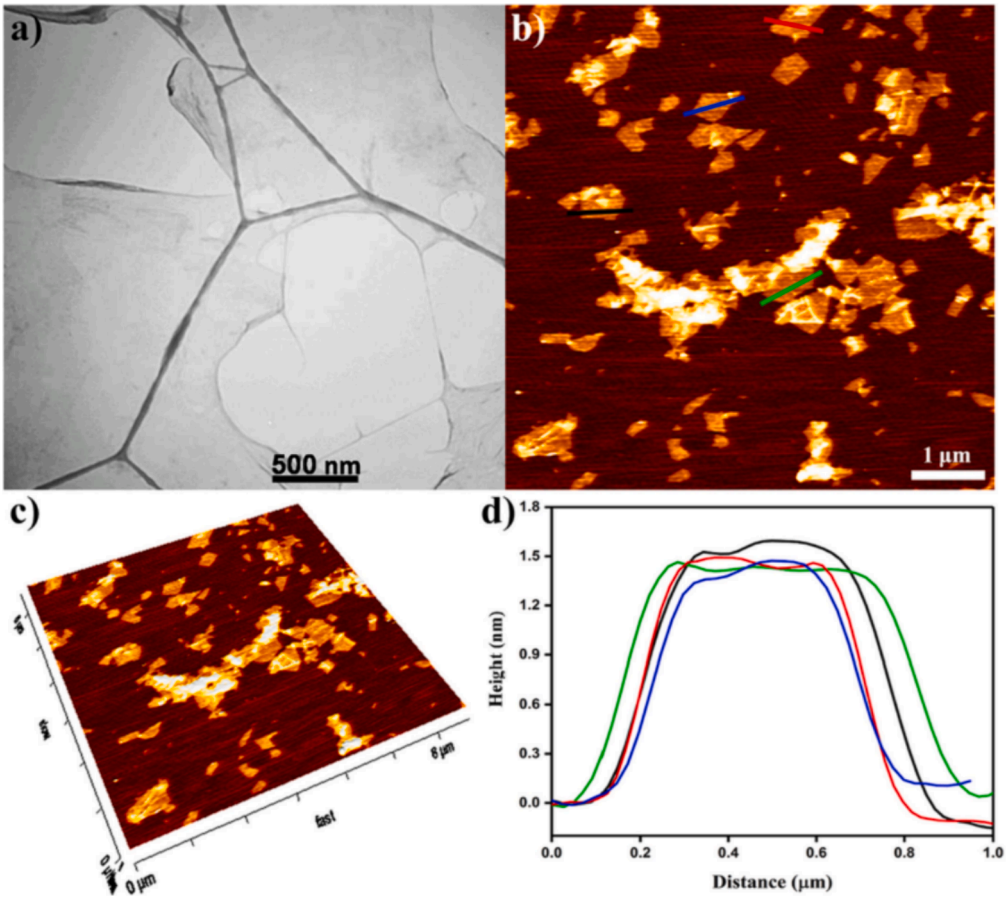

Fig. 6. TEM and atomic force microscope (AFM) analysis of morphology and microstructure of GO synthesized from graphite for utilization in colorimetric PH indicator based on soybean polysaccharides and grape skin anthocyanin. TEM image shows flexible and transparent GO sheets with a few wrinkles on their surface (a). AFM image of several GO sheets and its 3D topographical micrograph (b, c). and the height chart of GO nanosheets (d). Reprinted with permission from [71].

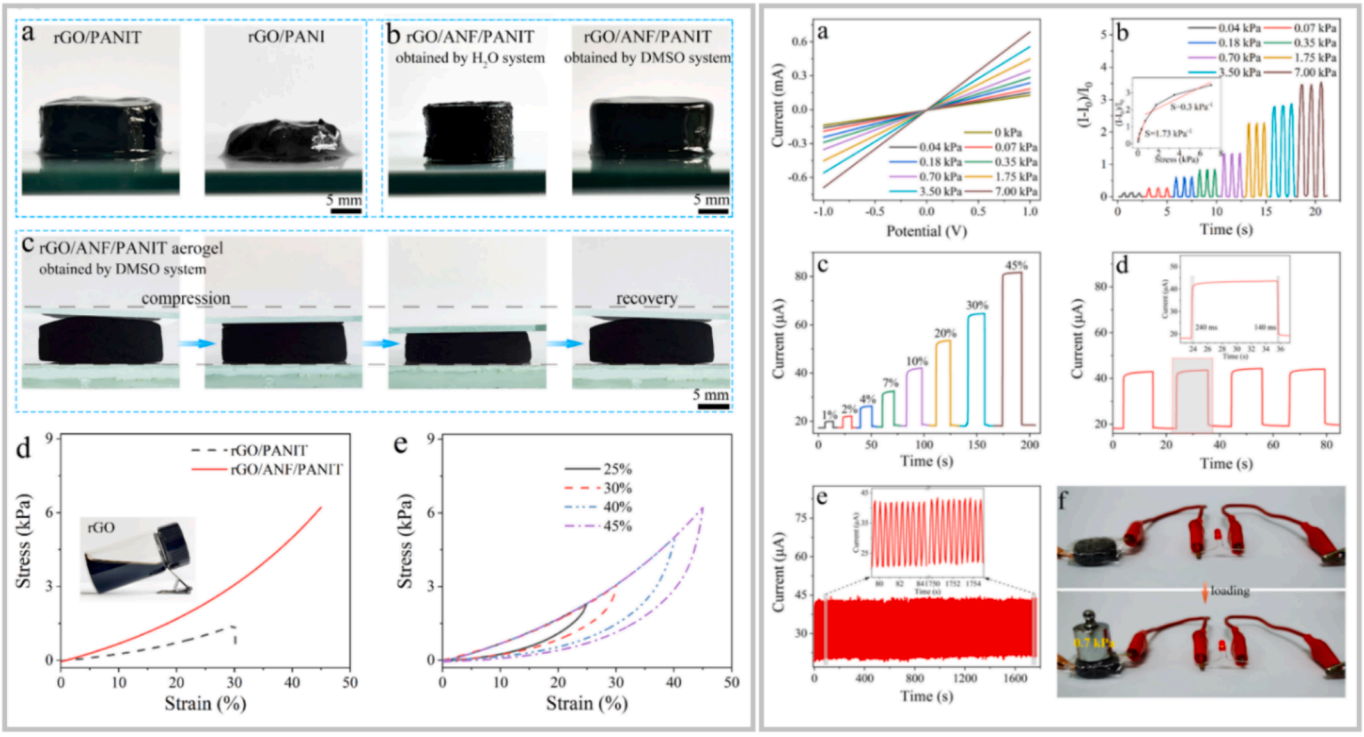

Fig. 7. Left side;(a) photographs of rGO-based gels obtained through different combinations; polyaniline nanotube (PANIT) compared to the polyaniline nanoparticle (PANI) could interconnect the adjacent graphene sheets to significantly reinforce the composite gels. (b) the more solid and brittle rough surface of rGO/ANF/PANIT hydrogel using the H_2O system compared to gel in the DMSO system resulted in a smaller volume of larger density. (c) Analysis of the compression and recovery dynamics of rGO/ANF/PANIT aerogels produced through the DMSO system. (d) Presentation of the compressive stress–strain profiles for both rGO/PANIT and rGO/ANF/PANIT aerogels fabricated via the DMSO system (e) Examination of compression profiles for rGO/ANF/PANIT aerogels at various strain levels. Right side; Sensitivity characteristics of the rGO/ANF/PANIT aerogel pressure sensor: (a) I − V curves under different pressures. (b) Variation in relative current with increasing pressure. (c) Current variation under constant pressure at different strain levels. (d) Current variation under constant pressure at a compression strain of 10 % (e) Stability assessment of sensing properties at 10 % strain, (f) Response of LED luminance variation (at 2 V) with and without pressure (0.7 kPa) applied to the rGO/ANF/PANIT aerogel sensors. Reprinted with permission from [74].

4.1. Mxenes-based 2D materials

In recent years, there have been significant advancements in synthetic techniques, leading to the successful production of an increasing number of 2D materials beyond graphene. One of the most notable is a large family of 2D early transition metal carbides and/or nitrides, known as 'MXenes', which has quickly gained popularity [75–78]. MXenes are primarily produced by etching the A layers from MAX phases. The MAX phases are ternary carbides or nitrides that have a general chemical formula of $M_{n+1}AX_n$. In this formula, M represents an early transition metal, A is an element from group IIIA or IVA, X is either C or N, and n can be 1, 2, or 3. MAX phases have a layered hexagonal structure, where the $M_{n+1}X_n$ units and the A layers are stacked alternately. The bonds between the M and X elements are highly stronger than the bonds between the M and A elements. This allows for the selective removal of the A layers through a process called chemical etching, without damaging the M−X bonds. As a result of the chemical etching process, the $M_{n+1}X_n$ layers are weakly bonded and can be easily separated using sonication. Accordingly, the 2D materials that are produced through this process are known as MXenes. This name emphasizes the removal of the A layers from the original MAX phase, as well as their similarity to graphene in terms of their 2D structure. It's important to note that during the etching process, the surfaces of the $M_{n+1}X_n$ units are always covered with functional groups such as oxygen (=O), hydroxyl (–OH), or fluorine (−F). As a result, the chemical formula for MXenes can be summarized as $M_{n+1}X_nT_x$, where T_x represents the surface functional groups (Fig. 1**b**) [79].

MXenes are typically produced through a three-step process, as shown in Fig. 8. The first step in producing MXenes involves synthesizing layered MXene precursors, which derive their crystal structure from MAX ($M_{n+1}AX_n$) or non-MAX phase layered materials. In MAX materials, "A" refers to group 11–16 atoms such as Al, Si, or Ga. Non-MAX phase layered materials can have more than one "A" atomic layer (e.g., $M_{n+1}A_2X_n$) or carbide layers of A-elements (e.g., $M_nA_3X_{n+2}$). In the second step of producing MXenes, the "A" atomic layers are etched away, which exfoliates the precursors and produces weakly bonded MXene multilayers. During the etching process of the "A" atomic layers, the weaker M−A bonds are cleaved, relative to the M−X bonds. This results in undercoordinated M metallic surfaces that are rapidly saturated again through a reaction with T_x species from the etchant. In the third and final step of producing MXenes, the exfoliated multilayer MXene sheets are delaminated to produce single-to-few layered MXene sheets [80].

MXene sheets are typically created using top-down methods. This is due to the fact that the bonds between the M and A elements are relatively weak, while the bonds between the M and X ones are strong. During this process, the A layers are removed by using solutions containing either HF or HCl, which break the M−A bonds without affecting the M−X bonds [81]. Two common types of etchants used to produce MXene sheets are HF or their salts and LiF-HCl solutions (Table 2). Strong etchants, such as HF and their salts, tend to introduce fluorine functional groups and produce small flakes with many defects. On the other hand, mild etchants containing LiF and HCl create fewer fluorine groups and have a smaller number of defects [82]. The $M_{n+1}X_n$ layers that remain after the chemical etching process can be further separated into nano-sheets through a process called exfoliation [81]. Indeed, the MAX phase is composed of multiple layers of sheets. When etched, the thickness of the exfoliated layers varies, typically within the micron-scale range. Consequently, the exfoliated MXene nanosheets display

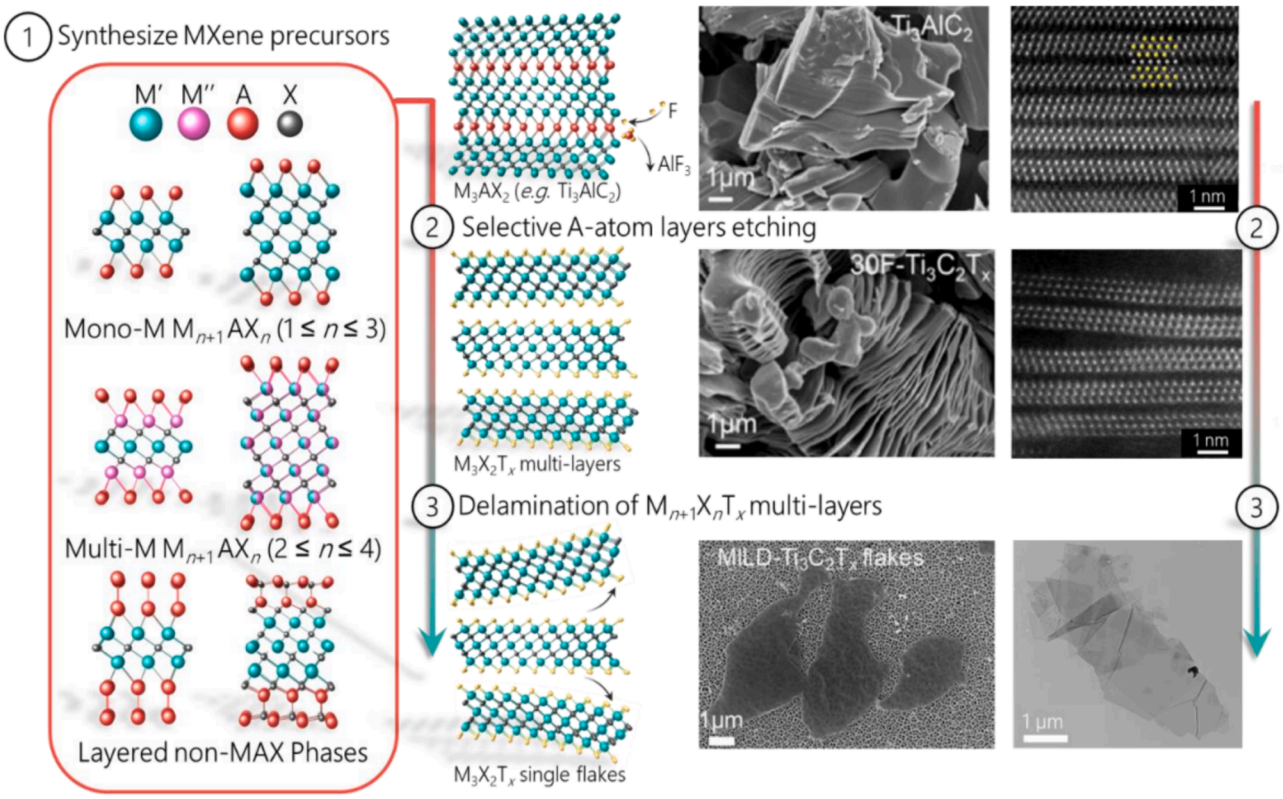

Fig. 8. The synthesis of MXenes involves several steps, with the etching of Ti_3AlC_2 MAX phase to produce $Ti_3C_2T_x$ MXene being used as an example. The first step in the process is the synthesis of precursors such as MAX ($M_{n+1}AX_n$) and non-MAX ($M_{n+1}A_2X_n$) phase layered materials (1). Non-MAX materials can contain more than one layer of "A" atoms, such as Mo_2Ga_2C, or an aluminum carbide layer between the MXene sheets, such as Al_4C_4 layers between Hf_3C_2 MXene sheets in $Hf_3Al_4C_6$. MAX phase materials can contain more than one "M" metal element, represented as M' and M''. These elements can be either structurally ordered, with M' and M'' as distinct atomic layers, or disordered solid solutions, with M' and M'' randomly distributed on the metal layers. In the second step of producing MXenes, the MXene precursors are etched to remove the "A" metal layers (2). This process exfoliates the precursors and yields weakly bonded MXene multilayers. In the third step, these multilayers are delaminated to form single sheets (3). In each row of the images, the SEM images are displayed on the left side, while the atomic resolution cross-sectional scanning TEM images are shown on the right side. For the $Ti_3C_2T_x$ single flakes shown in the bottom row, a plane-view TEM image is displayed on the right side, instead of a scanning TEM image. Reprinted with permission from [80].

Table 2
MXenes synthesized from various precursors and etchants.

MXenes	Precursors	Etchants	References
$Ti_3C_2T_x$	Ti_3AlC_2	HF	[88]
Ti_2CT_x	Ti_2AlC	HF	[89]
Ti_2NT_x	Ti_2AlN	HF	[90]
Ti_3CNT_x	Ti_3AlCN	HF	[91]
$Zr_3C_2T_z$	$Zr_3Al_3C_5$	HF	[92]
$Ti_3C_2T_x$	Ti_3AlC_2	HF	[93]
$Ti_3C_2T_x$	Ti_3AlC_2	HF	[93]
Mo_2CT_x	Mo_2Ga_2C	LiF + HCl	[94]
V_2CT_x	V_2AlC	NaF + HCl	[95]
$Ti_4N_3T_x$	Ti_4AlN_3	LiF + KF + NaF	[96]
Ti_3CNT_x	Ti_3AlCN	LiF + HCl	[97]
$Ti_3C_2T_x$	Ti_3AlC_2	NH_4HF_2	[98]
$Ti_3C_2T_x$	Ti_3AlC_2	NaOH	[99]

good transparency. It could be also noteworthy that LiF, KF, NaF, NH_4HF_2, and NaOH, have been explored as alternatives to remove the A layers. These etchants are used to avoid the hazardous nature and strong corrosion of hydrogen-based acids [83]. Some bottom-up methods, such as CVD method, have also been developed to produce MXene sheets. These methods allow for control over the size and shape of the particles, as well as the tribological properties and defects of the sheets [84–86]. One of the 2D MXenes that has been studied the most is $Ti_3C_2T_x$. It is produced by etching the Al layers in Ti_3AlC_2, followed by exfoliation [87].

MXenes offers two points for compositional changes: swapping elements at both the metal (M) and carbon/nitrogen (X) locations provides potential avenues to adjust MXenes' chemical, optical, electronic, or mechanical traits. In a study, the electronic and optical attributes of three interconnected binary solid-solution MXene combinations centered on Ti, Nb, and/or V in the M_2XT_x configuration were investigated [100]. This research introduced ways to manipulate the physical attributes of various MXenes through endless compositional possibilities in the M−site solid solutions. These systems formed consistent solutions at the M−site (Fig. 9**a**) and aim to understand the connection between composition and the MXenes' structural, electronic, and optical attributes. To comprehend the link between composition and electronic configuration, they employed DFT evaluations and X-ray Absorption Spectroscopy (XAS). Absorption readings were taken in the 200–1000 nm range, and electrical resistance was gauged from 10 to 300 K for each system. This research showed the potential to create countless new MXene combinations by altering the transition metal. This alteration offered enhanced control over MXene characteristics, making them adaptable for specific uses, such as blocking electromagnetic interference, storing energy, sensing applications, or color-changing films. The $Ti_{1.2}V_{0.8}CT_x$ was used as a representative to illustrate the crystal configuration and elemental layout. A 2D flake, transparent to electron beams, is visible in Fig. 9**b**. The hexagonal symmetry of the layers, with no noticeable lattice changes, was evident in the Fourier-filtered dark-field STEM image of the flake (Fig. 9**c**). The cross-sectional view of the flake revealed two bright layers, representing two metal layers, highlighting the M−C−M formation (Fig. 9**d**). Detailed EDS mapping

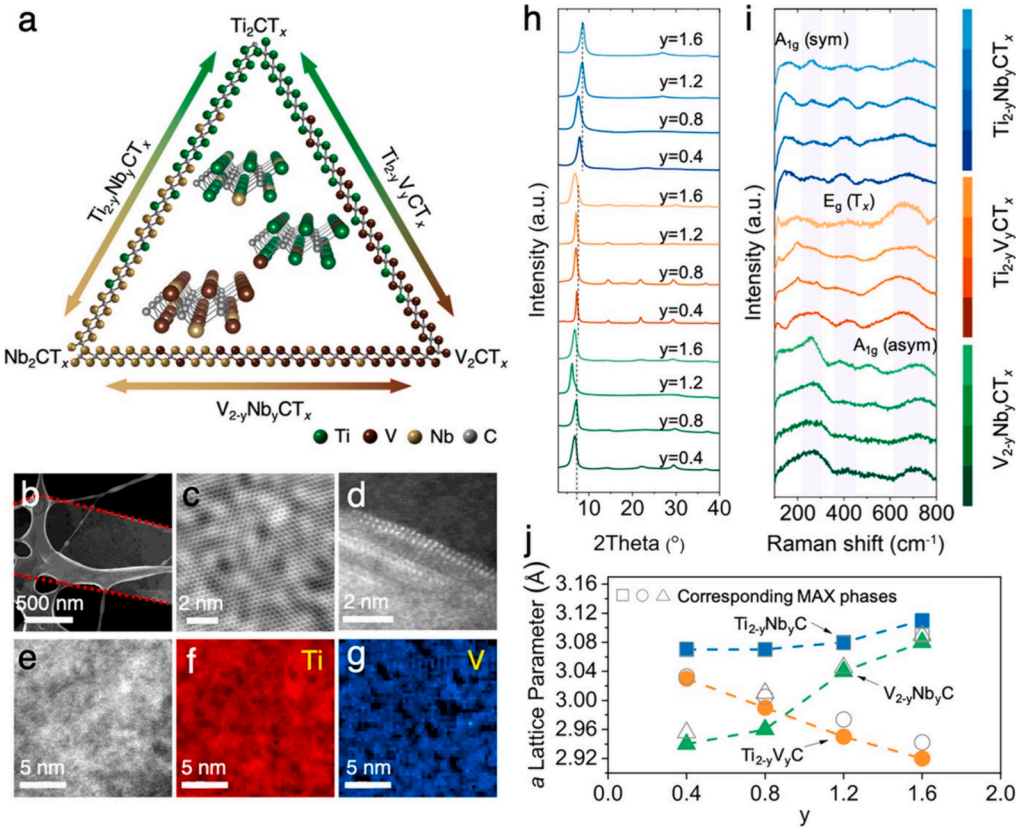

Fig. 9. Analysis of $M'_{2-y}M''_yCT_x$ MXenes in a solid-solution state. (a) A triangular representation of $Ti_{2-y}Nb_yCT_x$, $Ti_{2-y}V_yCT_x$, and $V_{2-y}Nb_yCT_x$ highlights the consistent solid solutions of M_2C-type MXenes. The dual arrows depict the color transition in MXene films as the M−site composition varies. The small images display the atomic layouts of these MXenes, indicating the metal element sequence used for DFT studies. (b) A STEM snapshot of a $Ti_{1.2}V_{0.8}CT_x$ MXene fragment, revealing its typical dimensions and form. (c) A refined dark-field STEM view of a $Ti_{1.2}V_{0.8}CT_x$ fragment along the [0 0 1] directional axis. (d) A side-view STEM capture of a $Ti_{1.2}V_{0.8}CT_x$ fragment, highlighting two bright atom layers (Ti/V layers). (e, f, g) STEM EDS maps of a $Ti_{1.2}V_{0.8}CT_x$ MXene, demonstrating the scattered placement of Ti and V. (h) XRD traces of all the MXene films examined, indicating the separated layers. (i) Raman readings of all MXene films, showcasing vibrational shifts with changing compositions. (j) The deduced lattice dimensions of pure $M'_{2-y}M''_yC$ MXenes, aligning closely with their respective MAX phase counterparts. Reprinted (reproduced) with permission from [100], Copyright 2020, American Chemical Society.

displayed an even spread of Ti and V atoms, confirming the sporadic placement of metal components (Fig. 9**e–g**). Both $Ti_{2-y}Nb_yCT_x$ and $Ti_{2-y}Nb_yCT_x$ MXenes possessed a crystal structure and elemental layout akin to $Ti_{2-y}V_yCT_x$. EELS assessments of $Ti_{2-y}V_yCT_x$ confirmed that the M−element composition aligned with the original $Ti_{2-y}V_yAlC$, and the elements were uniformly distributed. The DLS of $Ti_{2-y}V_yCT_x$ flakes indicated an intensity distribution average ranging from 140 to 520 nm.

MXenes has gained attention in food packaging due to their impressive properties. The combination of MXenes' inherent qualities and the crucial characteristics needed in packaging materials is what makes them a promising alternative. For instance, Ti_3C_2 MXene exhibits Young's modulus of approximately 333 ± 30 GPa, ranking among the highest for solution-processable 2D nanomaterials [101]. They are often integrated as fillers into polymers to enhance their mechanical properties and thermal stability [102,103]. The available functional groups on the MXenes' surfaces (O, OH, and/or F groups), provide them with excellent hydrophilicity. This characteristic makes them compatible with certain polymers commonly used in food packaging, which exhibit strong hydrophilic properties and feature numerous hydroxyl groups in their molecular structures.

In a study for the fabrication of an MXene-based sensor for ammonia (NH_3) sensing, the incorporation of gold nanoparticles (AuNPs) and core–shell nanoparticles of AuNPs with polyaniline (AuNPs@PANI) enhanced the sensing performance of the MXene sensor. $Ti_3C_2T_x$ MXene nanosheets were synthesized through the etching and exfoliation process of the Ti_3AlC_2 MAX. The electrode-based-sensor based on MXene and AuNPs@PANI composite (MXene/AuNPs@PANI) was fabricated by low-temperature ultrasonication (Fig. 10**a**). The outer layer of coated AuNPs was homogeneous with 21 nm diameter and core–shell AuNPs@PANI showed an integrated distribution in MXene (Fig. 10**b and c**). In the sensing process, MXene nanosheets showed several adsorption sites with ammonia molecules *via* surface functional groups (O, F, OH groups). PANI, as a p-type semiconductor, had high gas adsorption sites and high specific surface area. The incorporation of AuNPs promotes a more uniform dispersion of PANI and effectively modifies the gas adsorption rate while accelerating electron transfer. Whereas, with the introduction of AuNPs@PANI, more adsorption sites for ammonia were exposed owing to PANI's excellent ammonia sensing performance (Fig. 10**f**) [104].

4.2. *Silicate-clay-based 2D materials*

2D clay nanoparticles, comprising layered silicates also known as aluminum phyllosilicates with dimensions typically ranging from 10 to 100 nm in diameter and approximately 1 nm in thickness. These silicates contain metal oxides such as alkali earth metals, alkali metals, calcium, and other metal oxides. In addition, clay contains a small amount of organic elements [105,106]. Clay platelets represent 2D crystalline structures known for their remarkable strength, in-plane modulus, and distinctive structural anisotropy. These platelets occur naturally and can be widely found as layered nanosheets within soil mineral deposits. Utilizing clay platelets as a substitute for synthetic material components holds the potential to significantly support sustainable development—a feat that may not be possible for many other nanoparticles [107].

Clay ingredients can be classified into two types based on the

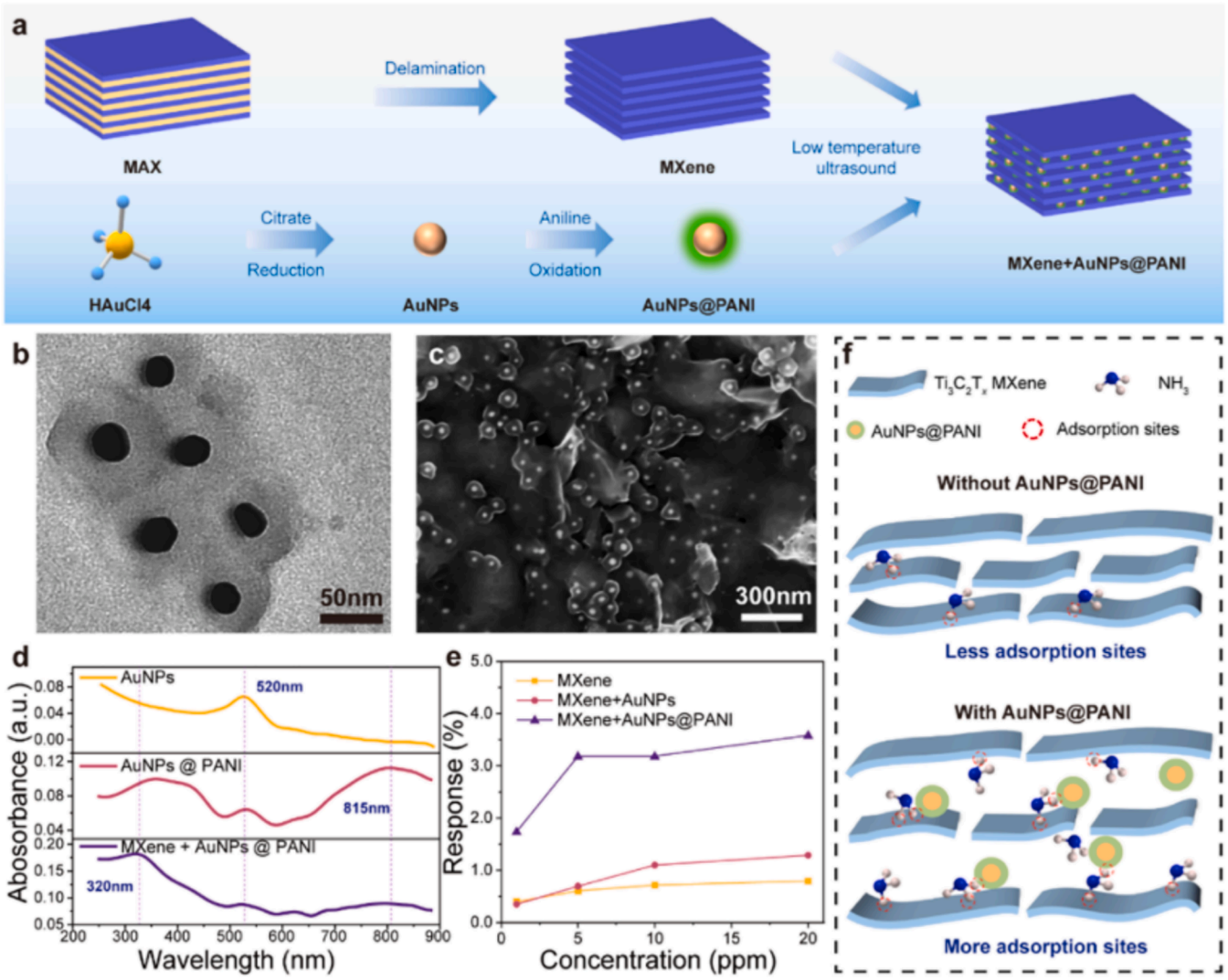

Fig. 10. Fabrication and analysis of the MXene/AuNPs@PANI sensor. (a) Synthesis of Ti_3C_2Tx MXene, gold nanoparticles (AuNPs), core–shell AuNPs with polyaniline (PANI), and MXene/AuNPs@PANI composite. (b, c) TEM and SEM images of MXene/AuNPs@PANI composite. (d) UV–Vis absorption spectra comparison of AuNPs, AuNPs@PANI, and MXene/AuNPs@PANI. (e) Evaluation of sensor responses among three variants: MXene alone, MXene/AuNPs, and MXene/AuNPs@PANI. (f) mechanism of ammonia sensing of MXene-based sensor. Reprinted with permission from [104].

arrangement of the alternating sheets of "SiO_2" and "AlO_6" units. The first type is 2:1 clay, which includes smectite and vermiculite. The second type is 1:1 clay, which includes kaolinite. Smectite clay minerals have a high aspect ratio due to their unique ability to intercalate and exfoliate. This makes them particularly effective as reinforcing fillers for polymers. Montmorillonite is one of the five major members of the smectite group of clay minerals, and it has a wide range of uses [28]. Montmorillonite clay is composed mainly of silicate layers that are 2:1 in ratio and only 1 nm in thickness. These layers consist of an alumina octahedral sheet that is sandwiched between two tetrahedral sheets of silica, with oxygen atoms being shared between them, as illustrated in Fig. 2**c**. Sodium and calcium ions are also present within the gallery or interlayer [108]. Clay materials that have a 1:1 structure are not commonly used in the creation of polymer nanocomposites. This is due to their inability to effectively intercalate and exfoliate, or because they are challenging to separate into individual layers. Due to the high charge density, the layers are packed tightly together, making it difficult or impossible for interlayer positive ions to hydrate or for polymer chains to penetrate the layers [28].

The hydrophilic nature of the clays and the covalent bonds that exist between the interlayers of the clay layers prevent most polymer matrices from reacting with or dispersing the clays. Additionally, electrostatic forces tightly hold the clay layer stacks together. In order to overcome this difficulty, clay particles are altered before being mixed into polymer matrices. The modification process involves the insertion of surfactants between the layers of clay, which increases the distance between them. By making certain changes, it is possible to make clay minerals repel water, allowing the modified clay to disperse very finely within polymer materials. The integration of silicate layers into organic and hybrid coatings can be accomplished by modifying clay particles with organic molecules that have two or more charged functional groups. This modification causes the clay particles to become "coated" with charges, leading to a repulsion between them. These particles can be easily dispersed in coating systems and bulk materials. Using colored modifiers, such as methylene blue, on the clays can result in colored nanocomposite coatings that have improved resistance to ultraviolet (UV) light and solvents [109]. This review does not cover a detailed explanation of the modification methods, their mechanisms, and the properties of the modified clays. For more information, readers can refer to the excellent review by researchers [105]. Such nanoparticles, prevalent in smart packaging and biomedical applications, demonstrate high drug loading capacity, aqueous stability, shear thinning behavior, and

improved interactions with biomaterials and cells [110].

5. Cutting-edge applications of 2D nanomaterials in the field of intelligent packaging

The utilization of 2D nanomaterials in intelligent packaging is a swiftly evolving domain that offers substantial potential for augmenting the functionality, safety, and sustainability of packaging materials. These nanomaterials, such as black phosphorus, graphene, GO, transition metal dichalcogenides (TMDs), and MXene, possess exceptional properties that make them ideal candidates for various applications in intelligent packaging [111,112]. By integrating sensors based on 2D nanomaterials into packaging materials, it becomes possible to monitor and track parameters such as temperature, humidity, gas concentration, and freshness of the packaged contents. This enables real-time information about the condition of the products and helps in maintaining optimal storage conditions [113,114]. Intelligent packaging with 2D nanomaterials can also incorporate indicators that provide visual cues about the quality or freshness of the packaged contents. These indicators can change color or display patterns in response to specific stimuli, allowing consumers to assess the quality of the products before purchasing [115]. Furthermore, labels and tags based on 2D nanomaterials offer enhanced functionalities such as wireless communication, anti-counterfeiting measures, and interactive features for consumers. They enable access to detailed product information, verification of authenticity, and personalized offers, improving consumer engagement and product traceability [116]. The versatility of 2D nanomaterials, coupled with their unique properties, opens up a wide range of possibilities for intelligent packaging applications. Ongoing research and development in this field hold the potential to revolutionize the packaging industry, leading to smarter, more efficient, and sustainable packaging solutions that benefit both consumers and the environment.

5.1. Sensors

One of the significant applications of 2D nanomaterials in intelligent packaging is the development of sensors. These sensors play a crucial role in monitoring and tracking of various parameters within the packaging environment [8,117]. By integrating sensors based on 2D nanomaterials, packaging can offer instantaneous updates regarding the state of the packaged contents. 2D material-based sensors can be fabricated to detect various changes within the package such as alternations in pressure, temperature, pH, gas, and humidity as well as bacteria and their metabolites produced during spoilage of food products or other analytes.

Chen et al. (2016) introduced a humidity sensor using a passive microwave substrate-integrated waveguide (SIW) resonator, which incorporated black phosphorus as a sensitive layer [118]. The sensor exhibited a remarkable sensitivity of 197.67 kHz/%RH, indicating its ability to accurately detect and respond to changes in humidity levels. This level of sensitivity is roughly 40 times higher than that observed in the SIW resonator without the presence of any sensing material. The findings indicated that the integration of a black phosphorus sensing layer into an SIW resonator could considerably improve the sensor's sensitivity to changes in humidity. Importantly, the use of black phosphorus-sensitive layers for sensor improvement resulted in only a marginal rise in dielectric losses. The suggested method is both budget-friendly and simple to incorporate, making it a viable option for integration with RF front ends in diverse monitoring applications.

In another study, amperometric biosensors were fabricated by constructing a nanocomposite film for detecting xanthine. The film consisted of separate components, including reduced expanded GO, GO-platinum, GO-gold, and GO-palladium, embedded in poly (glycidyl methacrylate-co-vinyl ferrocene). Xanthine oxidase (XO) was covalently immobilized to the surface of the electrode coated with the nanocomposite. By employing these customized nanocomposites and immobilizing XO on the surface, a comprehensive investigation was carried out to attain an optimum and ideal setup for detecting xanthine in actual samples. The GO-platinum-based nanocomposite electrode demonstrated the most superior performance in detecting xanthine. It showcased a sensitivity of 21.98 μA/μM, a linear range of detection spanning from 1 to 40 μM, an impressively low limit of detection at 0.003 μM, and a swift response time (2 s). To validate its effectiveness, the developed electrode was employed for assessing xanthine concentration in actual samples, specifically meat, and chicken, through measurements and analysis. The biosensor demonstrated exceptional performance and high precision in detecting xanthine in real samples over a span of 20 days. This makes it a practical and reliable approach to monitoring meat freshness control [112].

Detection of hydrogen peroxide (H_2O_2) is highly sought after due to environmental and health concerns. Numerous approaches have been devised for H_2O_2 monitoring, although many of them are limited by their reliance on complex instruments and high costs. In a recent study, Liu et al. (2022) introduced a novel approach using a label-free 2D photonic crystal (PhCr) sensor based on protein composite hydrogels including bovine serum albumin/ horseradish peroxidase (BSA/HRP) [119]. This sensor was designed to specifically detect H_2O_2 without the need for additional labels or markers. The 2-D PhCr BSA/HRP protein composite hydrogel sensor was created by gently cross-linking HRP and BSA proteins with glutaraldehyde. BSA functioned as a framework for HRP, which served as the molecular component for detecting H_2O_2. When HRP decomposes H_2O_2, its heme group is inactivated, causing a conformational change in the protein hydrogel. This change results in a decrease in cross-linking density, leading to an expansion of particle spacing and a reduction in the Debye diffraction pattern of the 2D photonic crystals. The composite hydrogel sensors of the 2D PhCr BSA/HRP −75 protein were fine-tuned, resulting in a favorable linear range spanning from 8.8×10^{-6} to 60.6×10^{-6} M. Furthermore, the sensors displayed remarkable sensitivity, boasting a detection limit of 8.8×10^{-6} M. This pioneering method of sensor fabrication establishes a proof-of-principle for the utilization of proteins with limited lysine groups in the advancement of intelligent PhCr protein composite hydrogel sensors designed for the precise measurement of H_2O_2 concentration in liquid solutions. Moreover, this strategy lays the foundation for future advancements in the creation of protein-based organogel sensors with the potential to detect gaseous H_2O_2.

Gases, more especially ammonia, serve as a crucial indicator for assessing food spoilage levels. However, existing gas sensors for detecting ammonia face challenges such as inadequate sensitivity, selectivity, and automation, hindering their practical use in real-time and on-site food quality monitoring. To address these limitations, Zhang et al. (2022) proposed a novel approach that involves growing (0 0 1) TiO_2 on a 2D transition-metal carbide ($Ti_3C_2T_x$, MXene) to create a specialized sensing material [114]. This design capitalizes on the highly active (0 0 1) crystal plane of TiO_2, which generates efficient photogeneration upon UV irradiation. Simultaneously, $Ti_3C_2T_x$ acts as a reservoir for holes, facilitated by the Schottky junction formed at the TiO_2 interface, leading to the dissociation of electron-hole pairs and enhanced performance in detecting ammonia. To augment the sensor's capabilities, authors introduced UV light to facilitate electron excitation, leading to a 34-fold increase in sensitivity to ammonia (30 ppm) in the (0 0 1) $TiO_2/Ti_3C_2T_x$-based sensor compared to $Ti_3C_2T_x$ alone. Density functional theory (DFT) analysis additionally validates that the combined arrangement of the TiO_2 (0 0 1) surface and $Ti_3C_2T_x$ demonstrates the strongest attraction to ammonia adsorption. Additionally, the researchers have devised an integrated alarm system circuit that integrates near-field communication and a microcontroller system, enabling the detection of the decay process in shrimp, fish, and fresh pork. The schematic diagram outlining the integrated alarm system's overall operation is depicted in Fig. 11**a**. Upon the fish's perished, the sensor detects the level of ammonia released by the fish, which in turn transmits a resistance signal to the microcontroller. A smartphone equipped

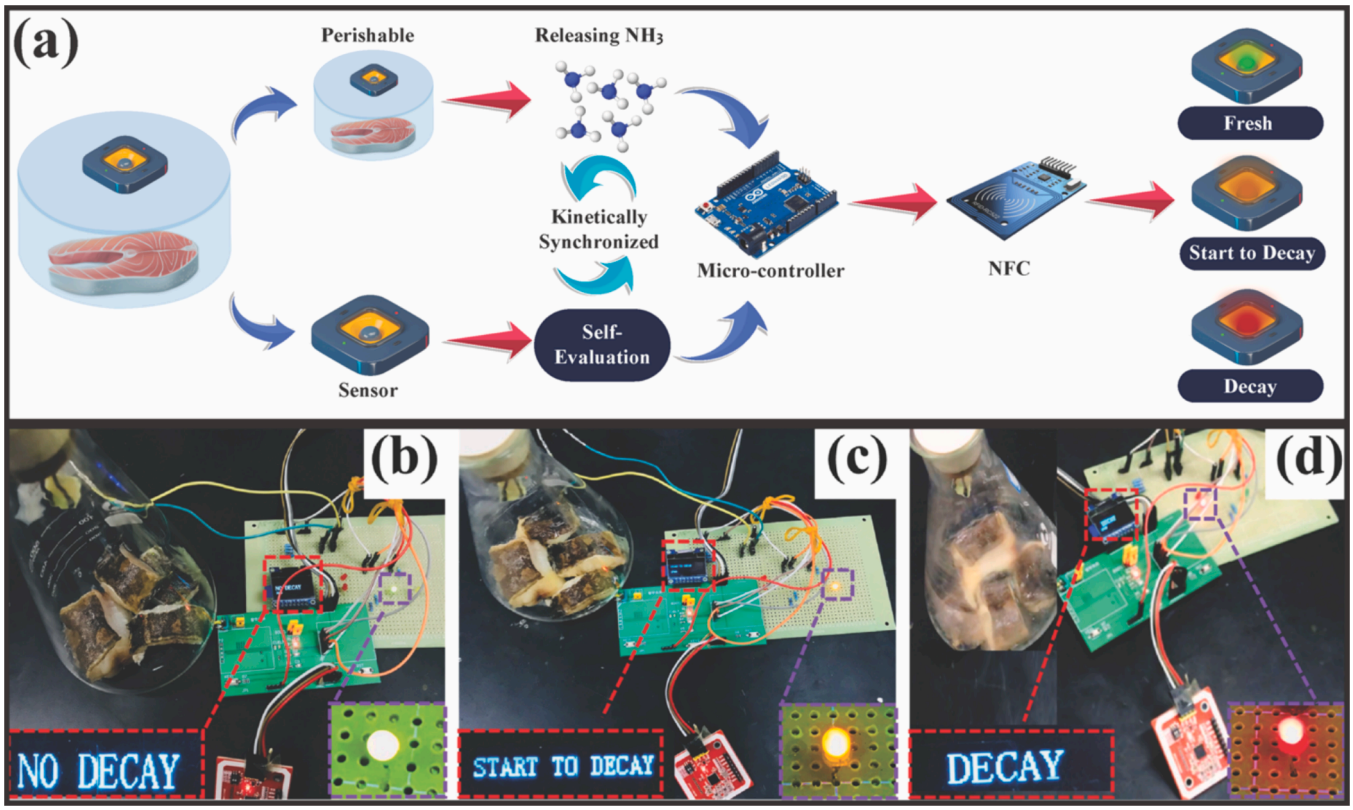

Fig. 11. (a) Schematic diagram of the integrated circuit alarm system. It showcases the real-time monitoring of the fish's present state, indicated as (b) "No deterioration," (c) "Early deterioration," and (d) "Advanced deterioration." Reprinted from [114] with permission from Elsevier Science Ltd.

with near-field communication (NFC) functionality is utilized to capture and interpret this signal. The integrated alarm system categorizes the decomposition process into three stages, indicated by "No deterioration" (green light), "early deterioration" (yellow light), and "advanced deterioration" (red light). Subsequently, the smartphone equipped with NFC capabilities is utilized to capture the signals. As the smartphone detects the sensor's signal, the current state of meat freshness is presented on the liquid crystal display (LCD) screen, accompanied by the activation of an indicator light, as illustrated in Fig. 11**b-d.** This novel sensing technology holds immense potential for revolutionizing food quality monitoring, overcoming the limitations of existing ammonia gas sensors, and facilitating efficient and automated on-site monitoring of food freshness.

Detecting multiple foodborne bacteria rapidly and sensitively without DNA amplification remains a significant challenge. 2D materials have also shown promising applications in biosensing devices. To address this, Shen et al. (2022) introduced an improved surface-enhanced Raman scattering (SERS) sensing strategy for directly detecting bacteria in 3 different food samples (grape juice, carrot juice, and skim milk), utilizing an immunochromatographic assay (ICA) with multiplex analysis capability and high sensitivity [120]. In their approach, they developed multifunctional nanosheets consisting of GO coated with a gold shell (GO@Au). These nanosheets were employed as a 2D film-like SERS label, offering excellent stability, a large surface area, and superior SERS activity. Unlike conventional spherical nanotags, the antibody-conjugated GO@Au nanosheets efficiently and promptly adhered to bacterial cells, enhancing the dispersibility of bacteria-nano label complexes on the ICA strips and generating numerous stable hotspots for SERS signal amplification. By combining the GO@Au labels with the ICA system, the researchers achieved multiplex and highly sensitive detection of three foodborne pathogens (*Salmonella typhimurium, Escherichia coli* O157:H7, *Staphylococcus aureus*) in a single test. The biosensor demonstrated low detection limits (10, 10, and 8 cells/mL) and a short time (approximately 20 min) for detection. Importantly, the fabricated biosensor exhibited excellent accuracy and stability when tested with different food samples, making it a desirable tool for rapid bacteria identification.

In brief, the utilization of 2D nanomaterials in advanced sensing applications offers a paradigm shift in the field of technology. With their unique properties, including high sensitivity, large surface area, and excellent stability, 2D nanomaterials have enabled the development of highly efficient and compact sensors. These sensors are able to revolutionize various industries by providing precise detection, real-time monitoring, and analysis of diverse parameters. As research in this area continues to progress, we can anticipate further advancements and the integration of 2D nanomaterials into a wide range of sensing devices, contributing to enhanced accuracy, reliability, and efficiency in numerous fields.

5.2. *Colorimetric/Visual indicators*

Intelligent packaging with 2D nanomaterials can incorporate indicators that provide visual cues about the quality or freshness of the packaged contents. These indicators are designed to change color or display patterns in response to specific stimuli [111]. 2D materials are frequently utilized to augment such types of indicators or act as either fluorescent emitters or effective fluorescence quenchers in the creation of diverse optical biosensors relying on fluorescence methodologies [17].

pH-sensitive indicators have demonstrated promise in different industrial sectors as a result of their quick response time and advantageous mechanical characteristics [121–123]. For instance, pH-sensitive sensors using nanofibrous membranes fabricated through electrospinning of a combination of poly 2-acrylamido-2-methylpropanesulfonic acid (PAMPS), polyurethane and GO, and indicator dyes. The ratio of hydrophilic polymer and GO concentration on the sensors' response time was then assessed. The solution tests across a wide pH range (1 to 8) and

vapor tests at three pH levels (1, 4, and 8) were performed and the color change was quantified using UV–vis spectroscopy to calculate the total color difference. The SEM analysis verified the successful production of bimodal distributions of fiber diameters, wherein polyurethane showcased an average fiber diameter of 519 nm, while PAMPS measured 78 nm. As the concentrations of GO and PAMPS increased, there was a notable reduction in the response time of the sensing system. The hybrid nanofibrous membranes, combining hydrophobic and hydrophilic properties with GO, exhibited a rapid response to changes in solution pH and could detect pH variations in chemical vapor solutions within 7 s [115]. In a similar investigation, Zhao et al. (2022) developed pH-sensitive smart packaging films by incorporating carboxymethyl cellulose (CMC) as the matrix, GO as the enhancer, and anthocyanins as the color indicator [124]. By utilizing this formulation, they were able to enhance the barrier properties of the films against oxygen and water vapor, as well as improve their tensile strength. Specifically, the oxygen permeability, water vapor transmission rate, and tensile strength were improved from their initial values to more favorable levels. The interaction between CMC and GO, facilitated by the electrophilic nature of carboxyl groups, led to a reduction in GO's surface energy and an improvement in the film's water contact angle from 88 to 142° indicating more hydrophobic surface of the indicator. Furthermore, the CMC/GO/anthocyanin composite indicator demonstrated high biodegradability and exhibited a visible color change in response to volatile ammonia and pH buffer solutions. These color changes were observable to the naked eye and were highly correlated with the total volatile basic nitrogen (TVB-N) levels and pH values. This suggested that the potential of the obtained films in smart packaging and gas/pH-sensing indicators, aiming to monitor and preserve the freshness of protein-based products.

Colorimetric indicators have also shown potential in modified atmosphere packaging (MAP) systems to detect the gas balance disturbances within the MAP package. In this regard, Huang et al. (2018) developed a convenient and visually detectable oxygen indicator to monitor the preservation state of MAP and control the reaction rate during the restoration phase [125]. This indicator was based on a composite of GO and titanium oxide, incorporating methylene blue, glycerol, PVA, and hydroxyethyl cellulose. The GO/titanium oxide nanocomposite synthesis involved a modified Hummers synthesis of GO, followed by hydrothermal treatment with butyl titanate, eliminating the need for a reducing agent. Performance tests utilizing UV–Vis spectroscopy and CIElab demonstrated that the indicator exhibited pseudo-first-order kinetics of methylene blue for the detection of O_2 in MAP. Notably, the findings indicated that the detection of MAP integrity loss is feasible, allowing consumers to make easy judgments based on the color of the indicator, with blue indicating damaged packaging. Furthermore, by adjusting the concentration of methylene blue, the reaction time of the indicator during the recovery stage could be controlled due to the pseudo-first-order kinetics.

To summarize, the application of 2D nanomaterials in packaging indicators has brought significant advancements to the field of intelligent packaging. These nanomaterials offer enhanced sensitivity, selectivity, and real-time monitoring capabilities for parameters like pH, gas composition, and product freshness. With further research, these advancements have the potential to enhance product safety, prolong shelf life, and instill consumer confidence in packaged goods.

5.3. Wireless tag

Another application of 2D nanomaterials in intelligent packaging is the development of labels or tags to provide valuable information, track, and trace capabilities, or even interact with consumers. These sensor tags possess the ability to independently monitor the conditions of packages, eliminating the need for manual involvement. They can be easily affixed to packages for wireless detection and recording of their condition, thereby improving supply chain visibility, particularly for products with security concerns [111].

The fabrication of the graphene-based wireless gas sensor involved the application of GO ink *via* inkjet printing onto organic paper or Kapton substrates. Following the introduction of ammonia gas, the electrical resistance underwent a rapid acceleration within the initial minutes, indicative of quick detection capabilities. This sensor material exhibited a 6 % normalized resistance change within 15 min of exposure to a concentration of 500 ppm. Furthermore, the rGO thin films demonstrated 30 % material recovery within 5 min without the need for high temperature or UV treatments. Besides, the rGO sensor displayed distinctive sensitivity characteristics when exposed to 0.1 % CO gas, however, the sensitivity was comparatively lower than that observed for ammonia gas [126].

In another study, the dielectric property of GO has been harnessed for the development of a wireless humidity sensor in the form of a radio-frequency identification (RFID) tag. The RFID sensor was fabricated by coating a printed graphene antenna with a layer of GO using screen printing. The resonance frequency and backscattering phase of this GO/graphene antenna were responsive to changes in surrounding humidity, allowing for detection by an RFID reader (24). In a similar study, a disposable humidity sensor was fabricated on various paper substrates (glossy, matt, and sylvicta) using screen printing with graphene-carbon ink. This sensor operated based on a resistive sensing mechanism. The humidity sensor exhibited promising sensing performance, showing a resistance change of approximately 12.4 Ω/%RH across a wide humidity range of 25–91.7 %RH. Notably, the sensor demonstrated high flexibility, considerable stability (over 4 months), excellent repeatability (over 100 cycles), rapid response (around 4 s), and recovery time (around 6 s) [127].

Wireless paper tags have also been developed for monitoring the temperature and chemical status of food products. Laser-induced paper sensors (LIPS) were developed by modifying commercial biodegradable papers to a paper-based graphene electrode using straightforward laser processing, aimed at real-time monitoring of food status. In this study, laser-induced graphene (LIG) was generated on the commercial paper *via* photothermal pyrolysis induced by laser irradiation (laser irradiation of 100 mW and 10 mm/s), without causing damage to the substrate, resulting in sheet resistance of 105 Ω/sq. The porous structure of the LIPS facilitated intelligent monitoring of necessary parameters such as gas concentration and temperature, allowing for early detection of food spoilage before consumption. The temperature and chemical gas coefficient of resistance were obtained as 0.15 % $℃^{-1}$ and 0.0041 % ppm^{-1}, respectively at the optimum laser irradiation conditions on the paper substrate. These LIPS were then utilized for monitoring the thermal state of water in a paper cup and assessing the chemical condition of pork and milk. The sensor data was seamlessly transmitted to the consumer's smartphone *via* constant wireless communication (Fig. 12) [128].

Strain-sensitive materials are another type of sensor that can be integrated into intelligent packaging. In this way, a composite sensor composed of pullulan/chitosan/alginate and graphene was fabricated to act based on the electrical characteristics of graphene [129]. In this study, few-layer graphene was generated through bath sonication of graphite in pullulan/ chitosan/alginate solutions. The resultant solution containing graphene was intended for use as an electrically conductive ink on the paper substrate in strain-sensitive applications. The chitosan-graphene combination exhibited the most favorable resistivity value (1.66×10^{-3} Ω·cm) and the highest sensitivity to strain (GF: 18.6). This interesting result highlighted the potential utility of chitosan-based conductive ink as a strain-sensitive material for next-generation food packaging.

In conclusion, the integration of 2D nanomaterials in paper-based tags offers tremendous potential for transforming industries, particularly in intelligent packaging. With their versatility and seamless integration into existing packaging materials, smart labels/tags with 2D nanomaterials present a scalable and unobtrusive solution for widespread implementation. Continued research in this field will likely drive the adoption of these advanced technologies, leading to improved

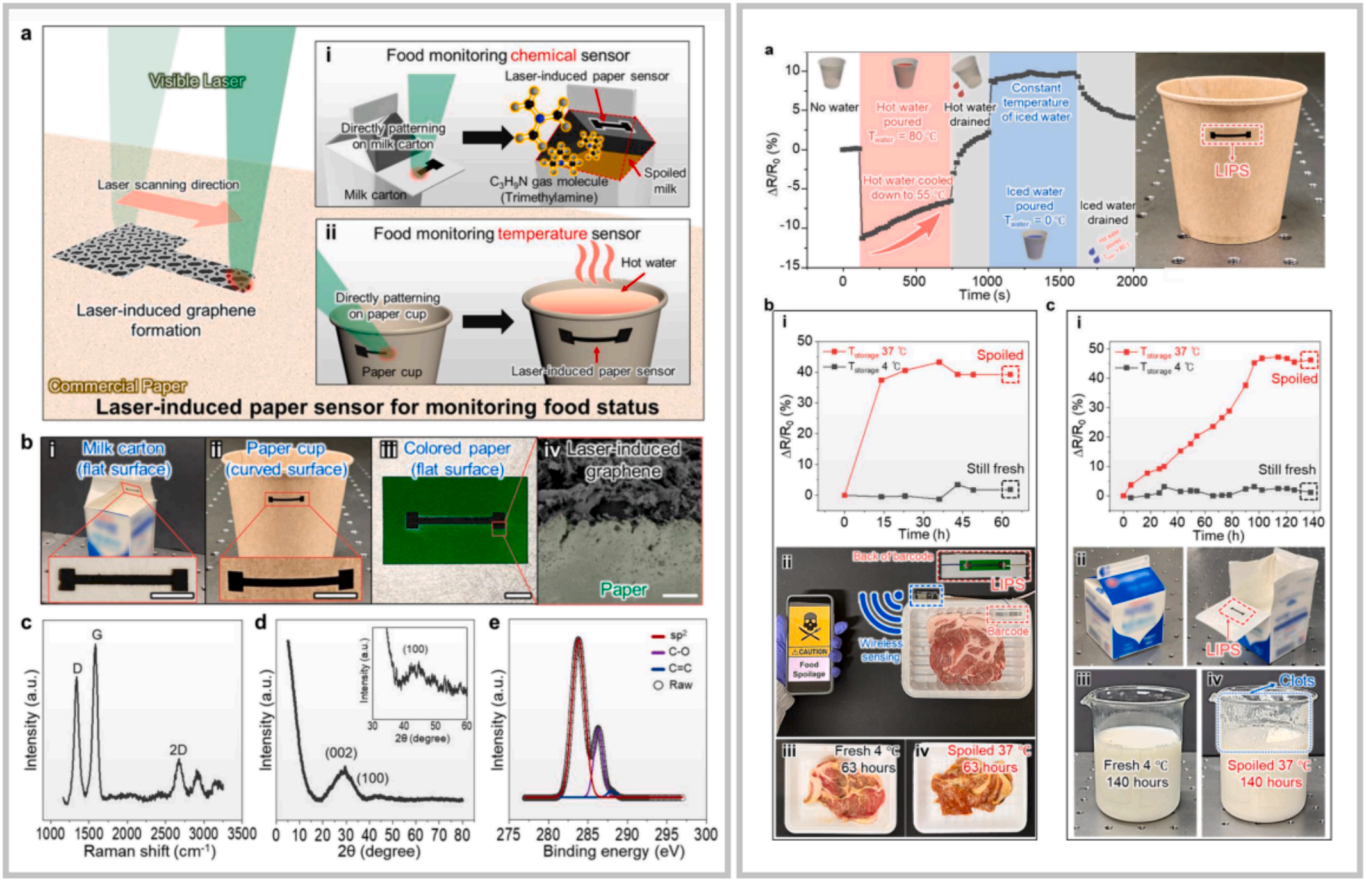

Fig. 12. Left side; (a) The process of fabrication of laser-induced paper sensor (LIPS) on commercial paper; (i) LIPS created (i) inside a milk carton for monitoring food chemicals and (ii) outside of a paper cup for monitoring food temperature. (b) Images of LIG patterns on commercial milk carton (i), paper cup (ii), and colored paper (iii) as well as its SEM image on colored paper (iv). (c,d,e) Raman, XRD, and XPS spectra of LIG. Right side; (a) Using LIPS for detecting water temperature in a paper cup by observing the response behavior of LIPS when hot/cold water is poured and drained. (b) Using LIPS for wireless monitoring of pork spoilage over time; (i) response of the LIPS by storing the pork at different temperatures (4 and 37 ℃), (ii) LIPS enclosed with the pork, and (iii, iv) pork preserved in the refrigerator (4 ℃) or warm oven (37 ℃) after 63 h. (c) The real-time wireless monitoring of milk spoilage (200 mL) using LIPS; (i) The response of LIPS for monitoring the status of milk stored at different temperatures (4 and 37 ℃). (ii) LIPS is patterned on the inner surface of a milk carton purchased from a local market, (200 mL), and (iii, iv) milk preserved in a refrigerator (4 ℃) and a warm oven (37 ℃) after 140 h representing visible solid clots for the spoiled milk. Reprinted with permission from [128].

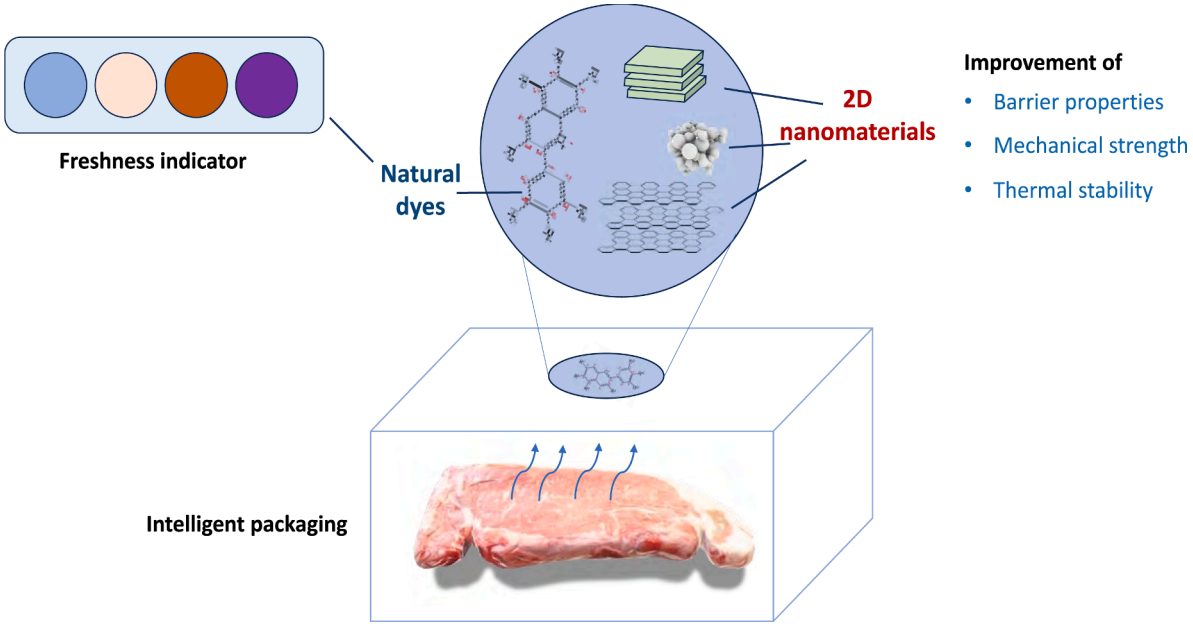

Fig. 13. Schematic overview of 2D nanomaterials' functions in intelligent food packaging.

product safety, enhanced supply chain management, and enriched consumer experiences in the near future.

6. Impact of 2D nanomaterials on the properties of smart packaging

It is well-known that the nanomaterials in composites improve various features of the final material, primarily barrier, mechanical, and thermal properties [117,130,131]. The intelligent or active packaging action arises mostly from other additives such as 2D materials or pH-responsive dyes as mentioned above. However, it is vital to keep in mind other, more conventional functions of packaging, namely mechanical and chemical resistance as well as desired barrier characteristics. These functions can be guaranteed and even improved by including nanomaterials in the synthesis protocol of the materials with potential intelligent packing properties. Both intelligent packaging and applicable nanotechnology are relatively young scientific fields. As a result, the literature providing a comprehensive description of intelligent packaging and other important properties is limited. However, the available data allows for drawing some general conclusions, noting trends, and predicting future perspectives in the area of 2D nanomaterial applications in intelligent food packaging. This section summarizes the available information and data related to the physical, barrier, and thermal properties of nanomaterial-containing smart packaging materials as shown in Fig. 13.

6.1. Barrier properties

Barrier properties represent the group of material features responsible for protecting the packed goods against UV radiation, moisture, water vapor, or gases [132]. These properties can be effectively tuned by the incorporation of the nanosized material into the polymeric structure.

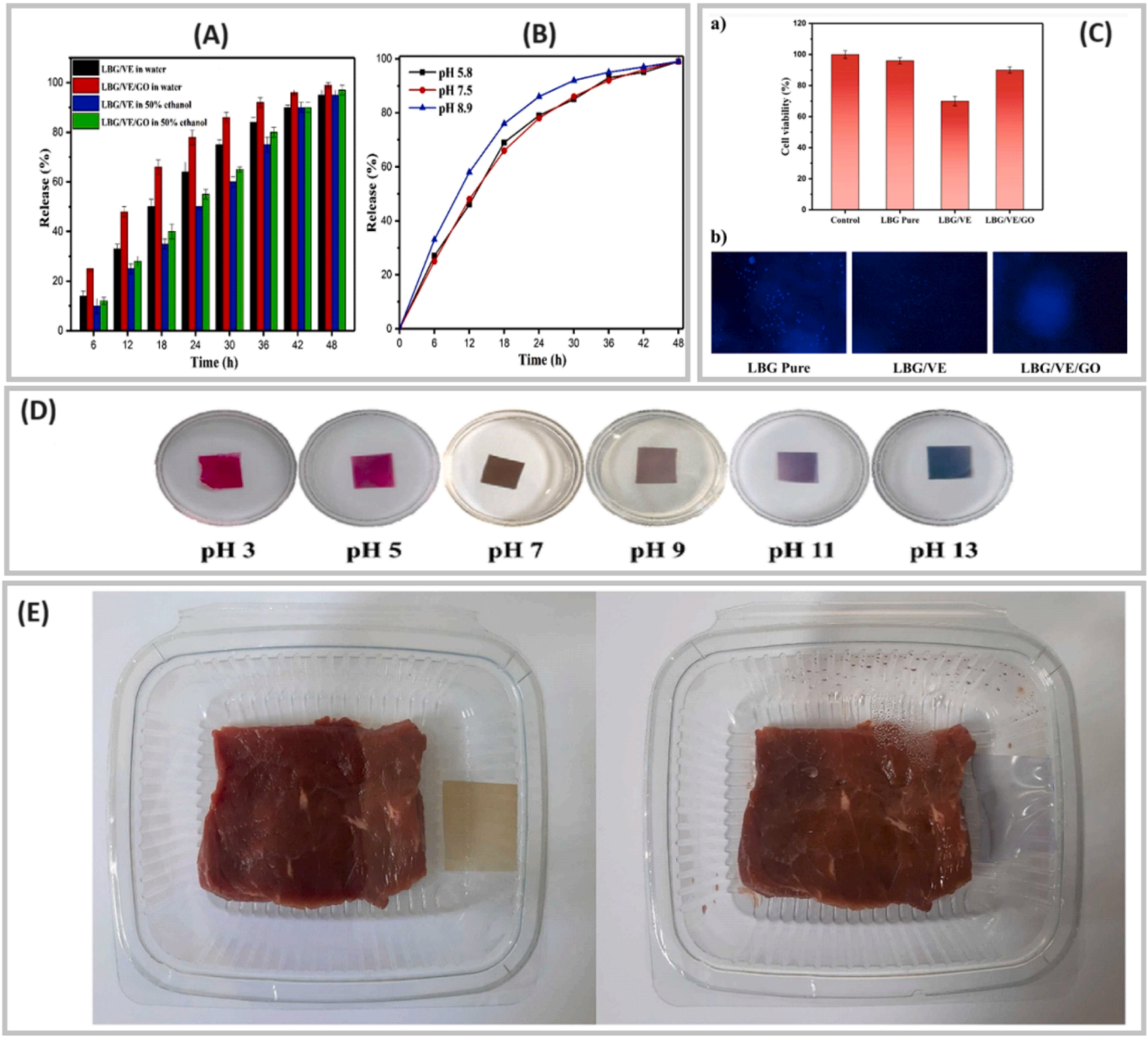

Fig. 14. The release profile of VE from LBG/VE film and LBG/VE/GO nanocomposite film to (A) the different food simulants and (B) the solutions with different pH values. (C) The cell viability results of HDF cells cultured on the film samples after 24 h. (b) Fluorescent microscopy images of DAPI stained nuclei of the cells after 12 h of culture on the fabricated films (b); (D) Color response of the LBG/VE/GO film at various pH values, and (E) Application of LBG/VE/GO film in monitoring meat freshness [133].

The 2D material structure is made up of multiple atomic layers that are connected by weak van der Waals forces. These materials provide a tortuous and extended path for gas/water vapor diffusion when they are incorporated into food packaging materials. As a result of this layered structure, gas molecules can pass through the packaging material at a lower permeation rate due to the extension of the effective diffusion path length. The nanoscale thickness and layering structure of 2D nanomaterials also result in a high surface area leading to higher interactions with gases/water vapor and absorbing them. By adhering to the surface of 2D nanomaterial-containing packaging, gas/water vapor concentration within the packaging is reduced, and thereby their permeation is slowed.

The optical properties of food packaging can be enhanced by 2D nanomaterials. Introducing compounds or materials containing chemical groups capable of absorbing visible and UV radiation typically leads to a decrease in transparency and an enhancement of UV resistance in the material. Sensitive food products can be protected from harmful UV radiation by packaging incorporated by 2D nanomaterials. They can protect food compounds from degradation and extend the shelf life of products exposed to UV light by acting as UV absorbers.

In a study, GO was incorporated into a film made of locust bean gum (LBG) and anthocyanin (*Viola* extract, VE) to develop a freshness controller for intelligent packaging [133]. The addition of GO did not significantly influence the WVP of the films. In general, the composite manifested lower WVP than the control film but this was ascribed to the interaction between the film matrix and VE. The oxygen permeability confirmed the "tortuous path" concept since the addition of VE and GO to the LBG matrix reduced the WVP by 38 and 74 %, respectively, in comparison to the neat film (Fig. 14). Similarly, Zhao et al. (2022) reported a promising material for real-time food freshness monitoring based on CMC enriched with anthocyanins as a pH-responsive compound and GO as a nanofiller [124]. The influence of GO addition on water vapor permeability (WVP) and oxygen permeability was systematically tested. The WVP is reduced by approximately 33–50 % depending on the amount of GO in the material. By adding the nanofiller, the oxygen permeability decreased to 50 % of the value noted for the graphene-free material, while it did not vary significantly with changes in the nanofiller content.

MXenes are promising materials for barrier and light absorption applications because of their layered structure and adjustable band gaps. In a recent study carried out by Zhang et al. (2022), ultrathin $Ti_3C_2T_x$ MXene nanosheets were prepared and utilized to create MXene/PVA composite films with enhanced UV shielding capabilities while maintaining high transparency [134]. These MXene/PVA composite films exhibited impressive UV shielding, with the 1.0 wt% $Ti_3C_2T_x$ MXene/PVA films blocking nearly 90 % of UV light. Remarkably, their visible-light transmittance held at above 55 %. The remarkable performance of these films was attributed to MXene's tunable band gap, ultrathin nature, layered structure, and excellent integration within the PVA matrix. Moreover, MXene/PVA exhibited exceptional water barrier properties. Additionally, films containing MXenes preserved product freshness and extended packaged products' shelf life. In another study, MXene ($Ti_3C_2T_x$) nanosheets were blended with polybutylene adipate-co-terephthalate (PBAT) through melt compounding to create smart food packaging materials. The findings revealed that MXene nanosheets significantly enhanced the biodegradable film's barrier properties. This improvement in gas barrier characteristics is attributed to the presence of $Ti_3C_2T_x$ nanosheets, which extend the effective diffusion path length for gases [135]. According to another study, a biodegradable composite film made of nanocellulose, MXene, and silver nanoparticles was designed and fabricated by Tang et al. (2023), resembled a nacre in its layered structure. The study's findings demonstrated that this compact structural arrangement, featuring reduced free volume, enhanced film gas diffusion pathways [136]. As a result, the nanocellulose/MXene/silver nanoparticles film exhibited remarkable barrier properties against oxygen, nitrogen, and volatile organic gases illustrating the effective role of MXene in improving nanocellulose films' barrier capabilities.

6.2. Mechanical properties

Ensuring the effective protection of the product is a fundamental task in packaging. As explained, the development of intelligent packaging is most commonly achieved through the modification of the polymeric matrix with various organic compounds. Such modifications often impact the mechanical properties of packaging materials in various ways. Over the last few decades, with the advancement of nanocomposites, it has been observed that incorporating nanofillers into certain polymer structures improves their mechanical properties. Therefore, applying this approach to intelligent food packaging can constitute a viable alternative. Tensile strength (TS), elongation at break (EAB), and Young's modulus (YM) are among the most commonly used parameters for the quantitative description of materials properties in terms of their mechanical resistance [117,137,138].

Eskandarabadi et al. (2019) investigated the effect of two nanofillers namely 2D montmorillonite (MMT) and zinc oxide (ZnO) separately and simultaneously on the TS of intelligent packaging materials based on ethylene vinyl acetate with the addition of anthocyanin [139]. The TS of the pure film matrix was 67 MPa whereas for the materials containing ZnO, MMT, and ZnO/MMT, it changed to 86, 70, and 54 MPa, respectively. This shows a slight but well-pronounced increase of the TS of material containing MMT (2D nanostructure) and an even higher effect for ZnO-modified material (3D nanostructure). However, the simultaneous incorporation of the nanofillers resulted in a reduction of the material's mechanical properties. This was ascribed to the change in polymer crystallinity due to the presence of both nanomaterials. Similarly, the incorporation of various concentrations of GO (1–6 % wt) to the polyvinyl chloride (PVC)-based humidity sensors changed the TS and EAB parameters as follows: 47, 70, 81, 41 MPa, and 225, 160, 95, and 66 % for the material containing 0, 1, 3, and 6 wt% of GO, respectively [140]. According to the results, the GO incorporation brought both positive and negative effects in terms of mechanical stability depending on the added amount. Moreover, there is some optimal GO content allowing for enhancement of the material TS whereas further increasing of the nanofiller content results in a decrease of the TS value. Mechanical tests of the ternary composite containing locust bean gum, *viola* anthocyanin, and GO confirmed the abovementioned observation and clearly showed the existence of some optimal limit for GO content. In this study, stepwise increasing the GO content in the locust bean gum matrix (without anthocyanin) from 0 to 0.5 wt% resulted in increasing the TS from 35 to 53-60nMPa and further addition of GO caused reverse changes to 30 MPa. Furthermore, the same trends were noted for the EAB and YM of the films. The incorporation of *viola* anthocyanin into the mixture of locust bean gum/ GO (with optimal GO content) led to the deterioration of the mechanical properties of materials, however, the values of TS and EAB were still higher than the neat locust bean gum (pure matrix) film, but the YM was slightly lower. Importantly, the mechanical properties of the material consisting of locust bean gum and viola anthocyanins only (without GO) were significantly worse than the pure matrix which justifies the application of the nanofiller in the intelligent packaging materials. Using GO as an enhancer in the CMC-based indicator containing anthocyanin enhanced the TS and YM, while EAB decreased. The mechanical parameters of the most promising material were equal to TS of 43 MPa, EAB of 8 %, and YM of 1.9 GPA whereas these parameters were obtained 13 MPa, 14 %, and 0.8 GPa, respectively, in the CMC indicator containing only anthocyanin. This constitutes further evidence of the validity of adding nanomaterials to composites dedicated to intelligent food packaging to ensure their mechanical strength.

6.3. Thermal properties

The modern food industry covers a wide spectrum of products being

processed in various ways including different temperature conditions. Some products are intended for storage at a reduced temperature, while others are processed at high temperatures within their final packaging, such as pasteurized and sterilized products. Due to this reason, the thermal properties of the packaging material cannot be overlooked in research which is reflected in the available literature. In the following cases, thermogravimetry has been used as a main tool for the evaluation of materials' thermal behavior [141–144].

The addition of 2D montmorillonite to the ethylene vinyl acetate nanocomposite resulted in a noticeable change in the thermal profile of the material. The application of this 2D nanomaterial allowed for an increase in the thermal stability of the composite by approximately 20 °C, which was observed as a delayed decomposition of the nanomaterial-doped material compared to the pure ethylene vinyl acetate film during heating. Another example of enhanced thermal properties of a nanocomposite in the presence of 2D nanomaterials is the CMC/gelatin composite modified with organoclay playing the role of 2D nanofiller [145]. In this case, the maximum thermal degradation of the CMC/gelatin film enriched separately with clay, anthocyanins, and *pistacia* leaf extract did not vary a lot, but the simultaneous application of these three components resulted in a synergistic effect of a positive shift of the degradation temperature by 13 °C. Fathi et al. (2022) observed, in turn, a positive influence of graphene addition on the thermal resistance of films consisting of locust bean gum and anthocyanin [133]. Films based on PVC and TCP containing different amounts of GO from 0 to 6 wt% were subjected to TGA (under air atmosphere) and the addition of 2D nanofiller resulted in the appearance of a new decomposition stage of material related to the presence of GO. The temperature of the main material decomposition peak shifted slightly towards a higher temperature, but this effect was relatively weak. The abovementioned examples of nanofiller-doped materials for intelligent food packaging have shown that this kind of modification can positively influence the thermal behavior of the material. In some cases, this was attributed to the presence of nano objects and in other cases to the occurrence of some synergistic effects.

However, deeper studies of the available literature suggest that this is not a common observation, and the application of 2D nanomaterials does not guarantee the improvement of the thermal properties. Zhao et al. (2022) reported almost no effect of graphene's presence on the thermal properties of CMC-based intelligent film which was related to the very small amount of the added graphene [124]. In another case, the pH-responsive material for intelligent food-packaging applications was synthesized as a mixture of natural and modified montmorillonite and a blueberry extract to make more stable intelligent packaging agents [146]. The authors observed that the addition of the blueberry extract as a pH indicator to the two kinds of montmorillonite resulted in decreasing its thermal properties but overall improved the stability of the extract. A similar pH-indicating system for application in intelligent food packaging was designed and tested by the same research group but in this case, the role of the intelligent component was played by anthocyanins. Like the previous example, the modification of montmorillonites with anthocyanins resulted in a decrease in the thermal behavior of the nanofiller. Noteworthy, the authors looked at the system from the perspective of montmorillonite properties, changing the perspective allows us to conclude that immobilization of anthocyanin in the clay structure results in its higher thermal stability which is a more promising option for food packaging applications.

6.4. Bioactive properties

Intelligent food packaging assumes the smart response of the packaging material to the chemical and physical changes in the product's internal and/or external environment. In certain instances, the inclusion of additives such as 2D materials can enhance the antimicrobial and antioxidative properties, thereby transforming the specific packaging solution into an active and intelligent option. Antioxidative and antimicrobial properties result in the active influence of the packaging itself on the quality of the packed product [147–149].

The antimicrobial efficacy of 2D nanomaterials arises from physical and chemical mechanisms. Physical damage involves processes that disrupt the physiological characteristics of microbial cells, including direct contact between the sharp edges of 2D nanomaterials and bacterial cell membranes, leading to membrane stress through cutting, insertion, lipid extraction, or pore formation [150] (Fig. 15**a**). Moreover, physical damage encompasses photo-thermal ablation, where the light-absorbing properties of 2D materials, coupled with pulsed laser action, convert near-infrared radiations (NIR) into local heat, effectively eliminating bacterial cells. Under NIR irradiation, 2D nanomaterials conduct heat and facilitate photo-thermally induced bacterial eradication (Fig. 15**b**). Mechanical wrapping, as another physical mechanism, induces membrane stress by enveloping bacterial cells, thereby isolating them from nutrients and causing cell death. In contrast, chemical damage arises from the reactivity of functional groups present on the surface of 2D nanomaterials. These materials promote the generation of reactive oxygen species (ROS) through oxygen adsorption at edges and defect sites, subsequently reduced by cellular enzymes like glutathione as a vital antioxidant. Glutathione is oxidized to glutathione disulfide serving as an indicator of intracellular redox state. Depletion of glutathione signifies elevated ROS levels, leading to oxidative stress and eventual bacterial toxicity (Fig. 15**c**) [151]. Various factors, such as the type of nanomaterial, concentration, and the microbe targeted, may affect the antimicrobial efficacy of 2D nanomaterials.

The incorporation of GO and rGO to the composite containing PVA and potassium chloride led to an enhancement of the bioactivity of the resultant composite [152]. The smart nanocomposite, containing 4 wt% GO as a dispersant, exhibited inhibitory activity against *Pseudomonas aeruginosa*, *Escherichia coli*, and *Campylobacter jejuni*. Additionally, the smart polymer nanocomposite, featuring 4 wt% rGO as a dispersant, demonstrated inhibitory activity against *Escherichia coli*, *Candida albicans*, and *Pseudomonas aeruginosa*, as evaluated using the good diffusion method. In addition, the antimicrobial properties of MXene ($Ti_3C_2T_x$) were investigated by incorporating it into composite films made from polylactic acid (PLA). The findings demonstrated that these composites effectively inhibited bacterial growth. Specifically, when tested against *Listeria*, a mere 0.5 wt% of MXene was sufficient to achieve a remarkable 99.999 % bactericidal activity, resulting in a six-log reduction. In the case of *Salmonella*, a concentration of 5 wt% was required to provide a significant 99.999 % bactericidal activity, corresponding to a five-log reduction [153]. In another research investigation, a new biopolymer composite film was engineered to possess exceptional antibacterial and antioxidant characteristics. This was obtained by incorporating MXene and tannic acid into a chitosan framework through hydrogen bonding and electrostatic self-assembly techniques. The outcomes of the study revealed an enhancement in the antibacterial and antioxidant attributes of the resulting chitosan-tannic acid/MXene film, rendering it suitable for various packaging applications. Additionally, experiments conducted on fruit preservation validated the composite film's ability to significantly extend the shelf life of bananas and grapes, due to its remarkable antibacterial and antioxidant properties [113]. Grande et al. (2017) carried out a study focused on the synthesis of nanocomposite films containing GO-chitosan and evaluated their efficiency as antimicrobial agents in food packaging [154]. The antimicrobial properties of these nanocomposite films were assessed using two bacterial strains: *E. coli* K-12 MG 1655 (Gram-negative) and *B. subtilis* 102 (Gram-positive). The findings showed that film content of 0.6 % GO exhibited the highest level of microbial inactivation against both *E. coli* and *B. subtilis*, with inactivation rates of 22.83 % and 54.93 %, respectively. In contrast, the control film (chitosan) displayed no noticeable antimicrobial properties. Consequently, the cross-linking of GO with chitosan significantly increased the antimicrobial characteristics of the films. According to another study, antimicrobial nanopackaging films were created through the addition of clove essential oil (CLO) at concentrations of 15–30 %

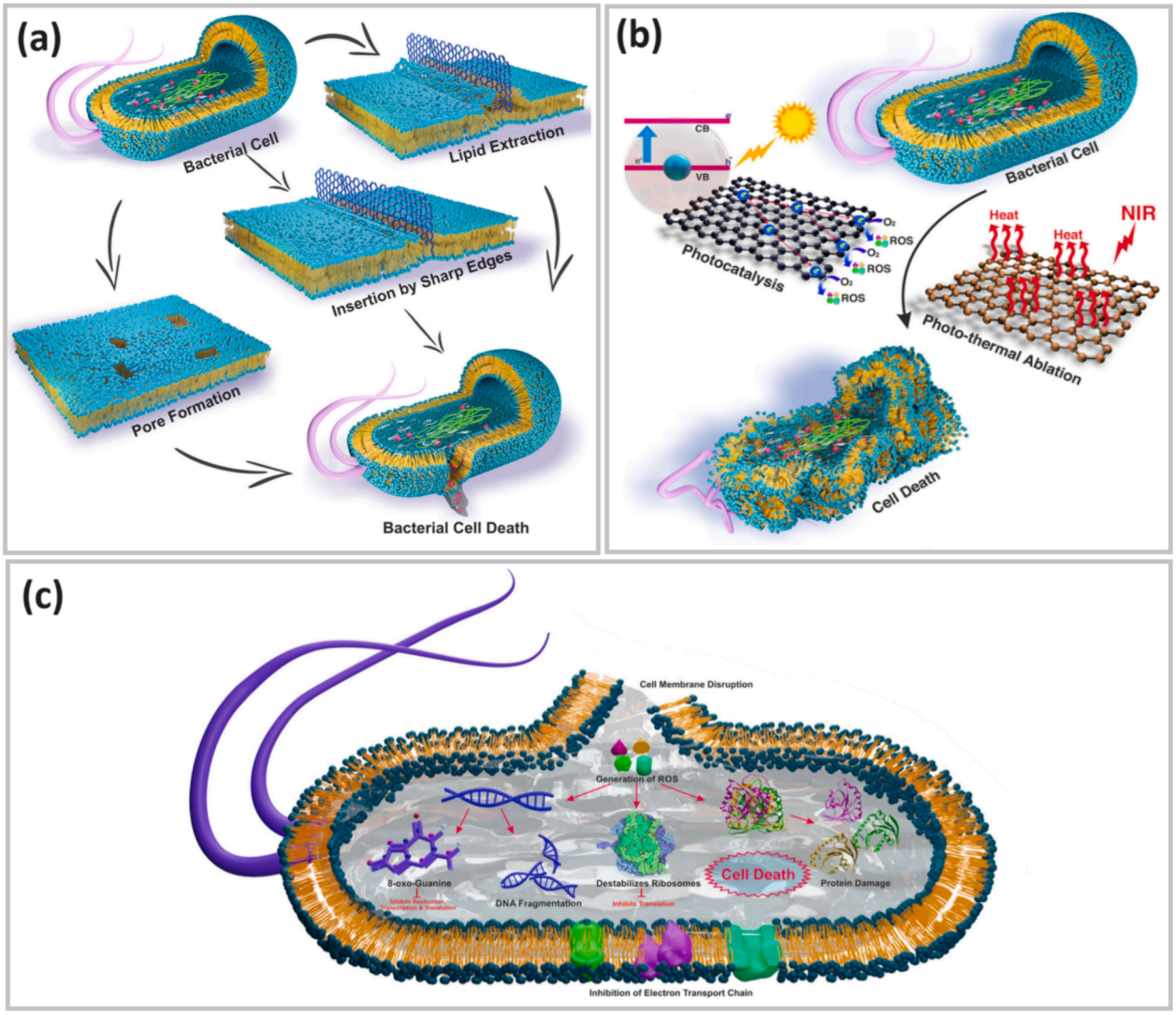

Fig. 15. Different mechanisms for antimicrobial activity of 2D materials; (a) Physical contact of sharp edges of 2D materials induces cell membrane stress through lipid extraction, insertion by sharp edges, and pore formation leading to the disruption of membrane, leakage of cytoplasmic content, and bacterial cell death. (b) Photocatalysis and photo-thermal ablation pathway for antibacterial activity of 2D materials by the generation of heat and reactive oxygen species (ROS); in the photo-thermal ablation process, 2D materials conducting heat under near-infrared (NIR) irradiation used for photothermally induced bacterial killing. Photocatalytic antibacterial action takes place as 2D materials generate ROS upon exposure to light exceeding their band gap. (c) The chemical mechanism of antibacterial activity encompasses the oxidative stress by ROS along with charge transfer processes contributing to the disruption of metabolic functions and eventual cell death. Reprinted by permission from [151].

(w/w) and GO nanosheets at 1 % (w/w) to PLA using a solution casting method. These composite films displayed remarkable antibacterial efficacy against *Staphylococcus aureus* and *Escherichia coli*. Consequently, they hold potential as active packaging materials for enhancing food safety and extending shelf life [155]. In summary, it can be concluded that 2D nanofillers provide favorable attributes to intelligent packaging materials.

7. Challenges and opportunities of 2D nanomaterials for intelligent packaging

Nanomaterials with 2D surfaces, ultra-thin, have gained considerable attention in recent years due to their unique properties. Smart food packaging applications can greatly benefit from 2D nanomaterials, which have superior properties such as high surface area, mechanical strength, and unique optical characteristics. The higher surface area can lead to more effective dispersion of 2D nanomaterials in food packaging materials. A tighter nanoparticle network can be created by this dispersion, improving the barrier properties of packaging [156]. This is essential for inhibiting oxygen, moisture, and other contaminants from affecting food shelf life. Moreover, the high surface area of 2D nanomaterials facilitates the effective binding of recognition molecules, providing the identification of food spoilage, temperature changes, or gas levels within the packaging. These nanomaterials can be customized to function as sensors and indicators in food packaging. The larger surface area also provides efficient distribution at a lower concentration. As a result, material usage can be reduced, making packaging more environmentally friendly and cost-effective.

A food package can be equipped with color-changing capabilities that respond to external factors, such as temperature, humidity, and gas concentration, by using 2D nanomaterials with specific optical properties. Food quality or safety can be determined by this color change. It is also important to note that 2D nanomaterials, such as graphene or GO, can significantly improve packaging materials' strength and durability. Adding these nanomaterials to polymers strengthens the matrix, improving its resistance to tearing, and a variety of physical stresses

during transportation and handling [157]. Despite 2D materials' potential and applications in various fields, there are some concerns that must mentioned for fully realized and used responsibly in different industries. In terms of product synthesis, the primary obstacle revolves around employing active exfoliation methods to generate 2D materials of the thinnest possible dimensions. The typical approach involves the use of potent acids, including those containing fluoride, to etch 2D materials. However, there is a necessity to explore environmentally friendly etching agents, for example laser etching, in MXene synthesis, as an alternative to the hazardous nature of hydrofluoric acid [158]. The issues connected with food packaging concerns are mainly the biocompatibility of used materials. Safety concerns arise regarding the migration of 2D nanomaterials into food products. Nevertheless, it is imperative to assess the quality of intelligent packaging through migration tests to ensure compliance with regulations and safeguard the well-being of consumers. The overall migration limit (OML) and specific migration limits (SML) serve as two indicators of material inertness and intentional additives. In line with European Union Commission Regulation No 10/2011 concerning food contact plastic materials, subject to regular updates based on new technical evaluations, plastic packaging must not surpass the OML threshold (set at 10 mg/dm^2 on the food contact surface or below 60 mg/kg). The potential 2D materials should undergo SML determination *via* compliance testing according to guidance outlined in the European Standard EN 13130–2005 [159]. The potential health risk associated with the 2D materials used in food packaging necessitates thorough safety assessments by regulatory bodies such as the Scientific Committee on Emerging and Newly Identified Health Risks [160]. Biocompatibility and immune response to 2D nanomaterials are strongly influenced by various factors, including their concentration, stability, size, functional groups, and shape. Among these factors, size and concentration are particularly important in determining biocompatibility [161]. Notably, the radial size of 2D nanomaterials determines their interaction with biological surfaces and their surroundings. Moreover, the size of 2D nanomaterials plays a critical role in their cellular absorption, biodistribution, circulation time, clearance routes, penetration through the blood–brain barrier, and overall performance efficiency. Therefore, the development of 2D materials with adjustable sizes can significantly enhance their application potential. Additionally, for the establishment of clinical translation and safety regulations, a thorough analysis of the toxicokinetic and toxicodynamic properties of 2D materials under physiological conditions is essential. The interactions at the nano-bio interface are strongly tied to 2D nanomaterial physicochemical characteristics. Nevertheless, accurately predicting the effects within biological systems remains a significant challenge [162]. In general, assessments of new nanomaterials' applications in food packaging are crucial, focusing on ecotoxicology, nanoecotoxicology, genotoxicology, human toxicology, and nanoparticle biodistribution.

In summary, the incorporation of 2D materials into food packaging offers a range of advantages. Depending on the requirement, these materials are customizable to meet specific needs and ensure food safety when they are biocompatible. However, their use in food packaging poses some challenges.

8. Conclusions

Intelligent food packaging systems prevent food waste by providing real-time information to consumers about the quality and condition of packaged food products, ensuring their safety and freshness. Hence, researchers are directing their efforts towards the development of innovative packaging systems. The integration of 2D materials has broadened the possibilities for creating cost-effective, environmentally friendly food packaging materials with enhanced performance and multiple functionalities. These remarkable materials, characterized by their high aspect ratios, hydrophobic nature, and extensive surface-to-volume ratio, play a key role in enhancing various aspects of composite packaging materials, including barrier properties, mechanical strength, thermal and antimicrobial attributes. Additionally, the physicochemical properties of 2D materials, such as high conductivity and catalytic activity, have enabled the way for their utilization in intelligent packaging. This application extends to indicators, sensors, tags, and smart labels, further enhancing the capabilities of food packaging in monitoring and maintaining the quality and safety of packaged products.

Current research and development in this field are creating the foundation for future innovations and applications. Moving forward, it is necessary to continue exploring the potential that 2D nanomaterials offer and their adaptability to diverse food products. Furthermore, a critical aspect of future research and development will involve addressing regulatory and safety concerns linked to 2D nanomaterial utilization in food packaging.

CRediT authorship contribution statement

Shima Jafarzadeh: Writing – review & editing, Writing – original draft, Project administration, Investigation, Conceptualization. **Majid Nooshkam:** Writing – original draft, Validation. **Zeinab Qazanfarzadeh:** Investigation, Writing – original draft. **Nazila Oladzadabbasabadi:** Writing – original draft, Visualization. **Przemyslaw Strachowski:** Writing – review & editing, Writing – original draft, Visualization, Validation. **Navid Rabiee:** Writing – review & editing, Validation. **Kamyar Shirvanimoghaddam:** Writing – review & editing, Validation, Investigation. **Mehdi Abdollahi:** Writing – review & editing, Validation, Investigation. **Minoo Naebe:** Visualization, Supervision.

Declaration of competing interest

The authors declare that they have no known competing financial interests or personal relationships that could have appeared to influence the work reported in this paper.

Data availability

No data was used for the research described in the article.

References

[1] S. Jafarzadeh, F. Ariffin, S. Mahmud, A.K. Alias, A. Najafi, M. Ahmad, characterization of semolina biopolymer films enriched with zinc oxide nano rods., Italian, J. Food Sci. 29 (2017).
[2] T. Mohammadi-Moghaddam, M. Kariminejad, S. Hadad, S. Jafarzadeh, D. Shahrampour, Physical properties antioxidant activity, and antimicrobial properties of edible film prepared from black plum peel extract as a valuable by-product of plum processing, J Food Chem Nanotechnol 9 (2023) 156–162.
[3] S. Jafarzadeh, M. Forough, V.J. Kouzegaran, M. Zargar, F. Garavand, M. Azizi-Lalabadi, M. Abdollahi, S.M. Jafari, Improving the functionality of biodegradable food packaging materials via porous nanomaterials, Compr. Rev. Food Sci. Food Saf. 22 (2023) 2850–2886.
[4] S. Jafarzadeh, Z. Yildiz, P. Yildiz, P. Strachowski, M. Forough, Y. Esmaeili, M. Naebe, M. Abdollahi, Advanced technologies in biodegradable packaging using intelligent sensing to fight food waste, (2024).
[5] P.R. Ghosh, D. Fawcett, S.B. Sharma, G.E.J. Poinern, Progress towards sustainable utilisation and management of food wastes in the global economy, Int. J. Food Sci. 2016 (2016).
[6] ood and Agriculture Organization of the United Nations (FAO), Food Wastage Footprint and its Effects on Natural Resources: Summary Report., 2013.
[7] K. Alirezalu, S. Pirouzi, M. Yaghoubi, M. Karimi-Dehkordi, S. Jafarzadeh, A. M. Khaneghah, Packaging of beef fillet with active chitosan film incorporated with ε-polylysine: An assessment of quality indices and shelf life, Meat Sci. 176 (2021) 108475.
[8] L.X. Mei, A.M. Nafchi, F. Ghasemipour, A.M. Easa, S. Jafarzadeh, A.A. Al-Hassan, Characterization of pH sensitive sago starch films enriched with anthocyanin-rich torch ginger extract, Int. J. Biol. Macromol. 164 (2020) 4603–4612.
[9] S. Jafarzadeh, M. Zargar, M. Forough, Renewable and recyclable polymeric materials for food packaging: a new open special issue in materials, Materials 15 (2022) 5845.
[10] S. Jafarzadeh, M. Nooshkam, M. Zargar, F. Garavand, S. Ghosh, M. Hadidi, M. Forough, Green synthesis of nanomaterials for smart biopolymer packaging: challenges and outlooks, J Nanostructure Chem (2023) 1–24.

[11] R. Syarifa, Y. Esmaeili, S. Jafarzadeh, F. Garavand, S. Mahmud, F. Ariffin, An investigation of the morphological, thermal, mechanical, and barrier properties of an active packaging containing micro-and nano-sized ZnO particles, Food Sci. Nutr. 11 (2023) 7373–7382.

[12] Y. Chen, Z. Fan, Z. Zhang, W. Niu, C. Li, N. Yang, B. Chen, H. Zhang, Two-dimensional metal nanomaterials: synthesis, properties, and applications, Chem. Rev. 118 (2018) 6409–6455.

[13] S.Z. Butler, S.M. Hollen, L. Cao, Y. Cui, J.A. Gupta, H.R. Gutiérrez, T.F. Heinz, S. S. Hong, J. Huang, A.F. Ismach, Progress, challenges, and opportunities in two-dimensional materials beyond graphene, ACS Nano 7 (2013) 2898–2926.

[14] M. Ahmadi, O. Zabihi, S. Jeon, M. Yoonessi, A. Dasari, S. Ramakrishna, M. Naebe, 2D transition metal dichalcogenide nanomaterials: advances, opportunities, and challenges in multi-functional polymer nanocomposites, J. Mater. Chem. A 8 (2020) 845–883.

[15] S.K. Tiwari, S. Sahoo, N. Wang, A. Huczko, Graphene research and their outputs: Status and prospect, J. Sci.: Adv. Mater. Devices 5 (2020) 10–29.

[16] L. He, X.-Q. Zhang, A.-H. Lu, Two-dimensional carbon-based porous materials: synthesis and applications, Acta Phys. Chim. Sin. 33 (2017) 709–728.

[17] M. Safarkhani, B. Farasati Far, E.C. Lima, S. Jafarzadeh, P. Makvandi, R.S. Varma, Y. Huh, M. Ebrahimi Warkiani, N. Rabiee, Integration of MXene and Microfluidics: A Perspective, ACS Biomater Sci Eng (2024).

[18] Y. Yu, J. Zheng, J. Li, L. Lu, J. Yan, L. Zhang, L. Wang, Applications of two-dimensional materials in food packaging, Trends Food Sci. Technol. 110 (2021) 443–457.

[19] S. Jafarzadeh, M. Golgoli, M. Azizi-Lalabadi, J. Farahbakhsh, M. Forough, N. Rabiee, M. Zargar, Enhanced carbohydrate-based plastic performance by incorporating cerium-based metal-organic framework for food packaging application, Int. J. Biol. Macromol. 130899 (2024).

[20] F. De Menna, J. Dietershagen, M. Loubiere, M. Vittuari, Life cycle costing of food waste: A review of methodological approaches, Waste Manag. 73 (2018) 1–13.

[21] S. Jafarzadeh, A. Alias, F. Ariffin, S. Mahmud, Characterization of Semolina Protein Film with Incorporated Zinc Oxide Nano Rod Intended for Food Packaging, Pol J Food Nutr Sci 67 (2017), https://doi.org/10.1515/pjfns-2016-0025.

[22] S. Jafarzadeh, A.K. Alias, F. Ariffin, S. Mahmud, A. Najafi, Preparation and characterization of bionanocomposite films reinforced with nano kaolin, J. Food Sci. Technol. 53 (2016), https://doi.org/10.1007/s13197-015-2017-7.

[23] M. Qiu, W.X. Ren, T. Jeong, M. Won, G.Y. Park, D.K. Sang, L.-P. Liu, H. Zhang, J. S. Kim, Omnipotent phosphorene: a next-generation, two-dimensional nanoplatform for multidisciplinary biomedical applications, Chem. Soc. Rev. 47 (2018) 5588–5601.

[24] J. Zeng, X. Ji, Y. Ma, Z. Zhang, S. Wang, Z. Ren, C. Zhi, J. Yu, 3D graphene fibers grown by thermal chemical vapor deposition, Adv. Mater. 30 (2018) 1705380.

[25] Y. Li, R. Wang, Z. Guo, Z. Xiao, H. Wang, X. Luo, H. Zhang, Emerging two-dimensional noncarbon nanomaterials for flexible lithium-ion batteries: opportunities and challenges, J. Mater. Chem. A 7 (2019) 25227–25246.

[26] G. Reina, J.M. González-Domínguez, A. Criado, E. Vázquez, A. Bianco, M. Prato, Promises, facts and challenges for graphene in biomedical applications, Chem. Soc. Rev. 46 (2017) 4400–4416.

[27] F. Seidi, A. Arabi Shamsabadi, M. Dadashi Firouzjaei, M. Elliott, M.R. Saeb, Y. Huang, C. Li, H. Xiao, B. Anasori, MXenes antibacterial properties and applications: a review and perspective, Small 19 (2023) 2206716.

[28] D.E. Abulyazied, A. Ene, An investigative study on the progress of nanoclay-reinforced polymers: Preparation, properties, and applications: A review, Polymers 13 (2021) 4401.

[29] N. Baig, Two-dimensional nanomaterials: A critical review of recent progress, properties, applications, and future directions, Compos. A Appl. Sci. Manuf. 165 (2023) 107362.

[30] M. Naebe, J. Wang, A. Amini, H. Khayyam, N. Hameed, L.H. Li, Y. Chen, B. Fox, Mechanical property and structure of covalent functionalised graphene/epoxy nanocomposites, Sci. Rep. 4 (2014) 4375.

[31] M.M. Abolhasani, S. Azimi, M. Mousavi, S. Anwar, M. Hassanpour Amiri, K. Shirvanimoghaddam, M. Naebe, J. Michels, K. Asadi, Porous graphene/poly (vinylidene fluoride) nanofibers for pressure sensing, J. Appl. Polym. Sci. 139 (2022) 51907.

[32] M. Tawalbeh, A. Al-Othman, A. Ka'ki, S. Mohamad, A. Al-Jahran, V. Unnikrishnan, O. Zabihi, Q. Li, K. Shirvanimoghaddam, M. Naebe, High Temperature Studies of Graphene Nanoplatelets-MOFs Membranes for PEM Fuel Cells Applications, Key Eng. Mater. 962 (2023) 93–98.

[33] K.V. Balaji, K. Shirvanimoghaddam, M. Naebe, Multifunctional basalt fiber polymer composites enabled by carbon nanotubes and graphene, Compos. B Eng. 268 (2024) 111070.

[34] R. Kumar, E. Joanni, R.K. Singh, D.P. Singh, S.A. Moshkalev, Recent advances in the synthesis and modification of carbon-based 2D materials for application in energy conversion and storage, Prog. Energy Combust. Sci. 67 (2018) 115–157.

[35] Y. Pan, L. Fu, Q. Zhou, Z. Wen, C. Lin, J. Yu, W. Wang, H. Zhao, Flammability, thermal stability and mechanical properties of polyvinyl alcohol nanocomposites reinforced with delaminated Ti3C2Tx (MXene), Polym. Compos. 41 (2020) 210–218.

[36] A. Barra, J.D.C. Santos, M.R.F. Silva, C. Nunes, E. Ruiz-Hitzky, I. Gonçalves, S. Yildirim, P. Ferreira, P.A.A.P. Marques, Graphene derivatives in biopolymer-based composites for food packaging applications, Nanomaterials 10 (2020) 2077.

[37] A.K. Sundramoorthy, S. Gunasekaran, Applications of graphene in quality assurance and safety of food, TrAC Trends Anal. Chem. 60 (2014) 36–53.

[38] K.P. Pramoda, H. Hussain, H.M. Koh, H.R. Tan, C.B. He, Covalent bonded polymer–graphene nanocomposites, J. Polym. Sci. A Polym. Chem. 48 (2010) 4262–4267.

[39] S.S. Varghese, S.H. Varghese, S. Swaminathan, K.K. Singh, V. Mittal, Two-dimensional materials for sensing: graphene and beyond, Electronics 4 (2015) 651–687.

[40] E. Loginova, N.C. Bartelt, P.J. Feibelman, K.F. McCarty, Factors influencing graphene growth on metal surfaces, New J. Phys. 11 (2009) 63046.

[41] C.-M. Seah, S.-P. Chai, A.R. Mohamed, Mechanisms of graphene growth by chemical vapour deposition on transition metals, Carbon 70 (2014) 1–21.

[42] Y. Zhang, L. Gomez, F.N. Ishikawa, A. Madaria, K. Ryu, C. Wang, A. Badmaev, C. Zhou, Comparison of graphene growth on single-crystalline and polycrystalline Ni by chemical vapor deposition, The Journal of Physical Chemistry Letters 1 (2010) 3101–3107.

[43] Y.S. Kim, J.H. Lee, Y.D. Kim, S.-K. Jerng, K. Joo, E. Kim, J. Jung, E. Yoon, Y. D. Park, S. Seo, Methane as an effective hydrogen source for single-layer graphene synthesis on Cu foil by plasma enhanced chemical vapor deposition, Nanoscale 5 (2013) 1221–1226.

[44] F. Wang, F. Wang, R. Hong, X. Lv, Y. Zheng, H. Chen, High-purity few-layer graphene from plasma pyrolysis of methane as conductive additive for LiFePO4 lithium ion battery, J. Mater. Res. Technol. 9 (2020) 10004–10015.

[45] S. Sunahiro, K. Nomura, S. Goto, K. Kanamaru, R. Tang, M. Yamamoto, T. Yoshii, J.N. Kondo, Q. Zhao, A.G. Nabi, Synthesis of graphene mesosponge via catalytic methane decomposition on magnesium oxide, J. Mater. Chem. A 9 (2021) 14296–14308.

[46] M.A. Azab, A.E. Awadallah, A.A. Aboul-Enein, S.A. Hassan, Single-step synthesis of graphene nanosheets-carbon nanotubes hybrid structure by chemical vapor deposition of methane using Fe-Mo-MgO catalysts, Fullerenes Nanotubes Carbon Nanostruct. 31 (2023) 109–119.

[47] C.-D. Kim, B.-K. Min, W.-S. Jung, Preparation of graphene sheets by the reduction of carbon monoxide, Carbon 47 (2009) 1610–1612.

[48] A. Chakrabarti, J. Lu, J.C. Skrabutenas, T. Xu, Z. Xiao, J.A. Maguire, N. S. Hosmane, Conversion of carbon dioxide to few-layer graphene, J. Mater. Chem. 21 (2011) 9491–9493.

[49] A.J. Strudwick, N.E. Weber, M.G. Schwab, M. Kettner, R.T. Weitz, J.R. Wünsch, K. Müllen, H. Sachdev, Chemical vapor deposition of high quality graphene films from carbon dioxide atmospheres, ACS Nano 9 (2015) 31–42.

[50] A. Guermoune, T. Chari, F. Popescu, S.S. Sabri, J. Guillemette, H.S. Skulason, T. Szkopek, M. Siaj, Chemical vapor deposition synthesis of graphene on copper with methanol, ethanol, and propanol precursors, Carbon 49 (2011) 4204–4210.

[51] M.H. Khan, M. Moradi, M. Dakhchoune, M. Rezaei, S. Huang, J. Zhao, K. V. Agrawal, Hydrogen sieving from intrinsic defects of benzene-derived single-layer graphene, Carbon 153 (2019) 458–466.

[52] C. Bautista, D. Mendoza, Multilayer graphene synthesized by CVD using liquid hexane as the carbon precursor, ArXiv Preprint ArXiv:1109.1318 (2011).

[53] A.A. Kaverzin, S.M. Strawbridge, A.S. Price, F. Withers, A.K. Savchenko, D. W. Horsell, Electrochemical doping of graphene with toluene, Carbon 49 (2011) 3829–3834.

[54] G. Kalita, S. Sharma, K. Wakita, M. Umeno, Y. Hayashi, M. Tanemura, Synthesis of graphene by surface wave plasma chemical vapor deposition from camphor, Physica Status Solidi (a) 209 (2012) 2510–2513.

[55] J. Qu, C. Luo, Q. Zhang, Q. Cong, X. Yuan, Easy synthesis of graphene sheets from alfalfa plants by treatment of nitric acid, Mater. Sci. Eng. B 178 (2013) 380–382.

[56] S. Sankar, H. Lee, H. Jung, A. Kim, A.T.A. Ahmed, A.I. Inamdar, H. Kim, S. Lee, H. Im, D.Y. Kim, Ultrathin graphene nanosheets derived from rice husks for sustainable supercapacitor electrodes, New J. Chem. 41 (2017) 13792–13797.

[57] M.S.A. Faiz, C.A.C. Azurahanim, Y. Yazid, A.B. Suriani, M.J.S.N. Ain, Preparation and characterization of graphene oxide from tea waste and it's photocatalytic application of TiO2/graphene nanocomposite, Mater. Res. Express 7 (2020) 15613.

[58] K. Shoueir, A. Mohanty, I. Janowska, Industrial molasses waste in the performant synthesis of few-layer graphene and its Au/Ag nanoparticles nanocomposites. Photocatalytic and supercapacitance applications, J. Clean. Prod. 351 (2022) 131540.

[59] R.V. Salvatierra, V.H.R. Souza, C.F. Matos, M.M. Oliveira, A.J.G. Zarbin, Graphene chemically synthesized from benzene at liquid–liquid interfaces, Carbon 93 (2015) 924–932.

[60] R. Negishi, H. Hirano, Y. Ohno, K. Maehashi, K. Matsumoto, Y. Kobayashi, Layer-by-layer growth of graphene layers on graphene substrates by chemical vapor deposition, Thin Solid Films 519 (2011) 6447–6452.

[61] G. Ruan, Z. Sun, Z. Peng, J.M. Tour, Growth of graphene from food, insects, and waste, ACS Nano 5 (2011) 7601–7607.

[62] J.K. Saha, A. Dutta, A review of graphene: material synthesis from biomass sources, Waste Biomass Valoriz. (2022) 1–45.

[63] C. Long, X. Chen, L. Jiang, L. Zhi, Z. Fan, Porous layer-stacking carbon derived from in-built template in biomass for high volumetric performance supercapacitors, Nano Energy 12 (2015) 141–151.

[64] Z. Wang, H. Ogata, S. Morimoto, J. Ortiz-Medina, M. Fujishige, K. Takeuchi, H. Muramatsu, T. Hayashi, M. Terrones, Y. Hashimoto, Nanocarbons from rice husk by microwave plasma irradiation: From graphene and carbon nanotubes to graphenated carbon nanotube hybrids, Carbon 94 (2015) 479–484.

[65] Y. Zhu, S. Murali, W. Cai, X. Li, J.W. Suk, J.R. Potts, R.S. Ruoff, Graphene and graphene oxide: synthesis, properties, and applications, Adv. Mater. 22 (2010) 3906–3924.

[66] D.G. Trikkaliotis, A.K. Christoforidis, A.C. Mitropoulos, G.Z. Kyzas, Graphene oxide synthesis, properties and characterization techniques: a comprehensive review, ChemEngineering 5 (2021) 64.
[67] G. Goncalves, P.A.A.P. Marques, C.M. Granadeiro, H.I.S. Nogueira, M.K. Singh, J. Gracio, Surface modification of graphene nanosheets with gold nanoparticles: the role of oxygen moieties at graphene surface on gold nucleation and growth, Chem. Mater. 21 (2009) 4796–4802.
[68] W. Gao, The chemistry of graphene oxide, Graphene Oxide: Reduction Recipes, Spectroscopy, and Applications (2015) 61–95.
[69] A.M. Dimiev, S. Eigler, Graphene oxide: fundamentals and applications, John Wiley & Sons, 2016.
[70] H. Moustafa, M.H. Hemida, M.A. Shemis, A. Dufresne, M. Morsy, Functionalized GO nanoplatelets with folic acid as a novel material for boosting humidity sensing of chitosan/PVA nanocomposites for active food packaging, Surf. Interfaces 41 (2023) 103229.
[71] A. Kafashan, H. Joze-Majidi, S. Kazemi-Pasarvi, A. Babaei, S.M. Jafari, Nanocomposites of soluble soybean polysaccharides with grape skin anthocyanins and graphene oxide as an efficient halochromic smart packaging, Sustain. Mater. Technol. 38 (2023) e00755.
[72] R. Tarcan, O. Todor-Boer, I. Petrovai, C. Leordean, S. Astilean, I. Botiz, Reduced graphene oxide today, J. Mater. Chem. C 8 (2020) 1198–1224.
[73] H. Yu, W. Guo, X. Lu, H. Xu, Q. Yang, J. Tan, W. Zhang, Reduced graphene oxide nanocomposite based electrochemical biosensors for monitoring foodborne pathogenic bacteria: A review, Food Control 127 (2021) 108117.
[74] Y. Zou, Z. Chen, X. Guo, Z. Peng, C. Yu, W. Zhong, Mechanically robust and elastic graphene/aramid nanofiber/polyaniline nanotube aerogels for pressure sensors, ACS Appl. Mater. Interfaces 14 (2022) 17858–17868.
[75] M.S. Bhargava Reddy, S. Kailasa, B.C.G. Marupalli, K.K. Sadasivuni, S. Aich, A family of 2D-MXenes: synthesis, properties, and gas sensing applications, ACS Sensors 7 (2022) 2132–2163.
[76] A. Parihar, N.K. Choudhary, P. Sharma, R. Khan, MXene-based aptasensor for the detection of aflatoxin in food and agricultural products, Environ. Pollut. 316 (2023) 120695.
[77] A. Rhouati, M. Berkani, Y. Vasseghian, N. Golzadeh, MXene-based electrochemical sensors for detection of environmental pollutants: A comprehensive review, Chemosphere 291 (2022) 132921.
[78] S. Ullah, F. Shahzad, B. Qiu, X. Fang, A. Ammar, Z. Luo, S.A. Zaidi, MXene-based aptasensors: Advances, challenges, and prospects, Prog. Mater Sci. 129 (2022) 100967.
[79] X. Zhan, C. Si, J. Zhou, Z. Sun, MXene and MXene-based composites: synthesis, properties and environment-related applications, Nanoscale Horiz. 5 (2020) 235–258.
[80] K.R.G. Lim, M. Shekhirev, B.C. Wyatt, B. Anasori, Y. Gogotsi, Z.W. Seh, Fundamentals of MXene synthesis, Nature, Synthesis 1 (2022) 601–614.
[81] M. Malaki, R.S. Varma, Mechanotribological aspects of MXene-reinforced nanocomposites, Adv. Mater. 32 (2020) 2003154.
[82] X. Shen, Q. Zheng, J.-K. Kim, Rational design of two-dimensional nanofillers for polymer nanocomposites toward multifunctional applications, Prog. Mater Sci. 115 (2021) 100708.
[83] X. Zhou, Y. Hao, Y. Li, J. Peng, G. Wang, W. Ong, N. Li, MXenes: An emergent materials for packaging platforms and looking beyond, Nano Select 3 (2022) 1123–1147.
[84] D. Geng, X. Zhao, Z. Chen, W. Sun, W. Fu, J. Chen, W. Liu, W. Zhou, K.P. Loh, Direct synthesis of large-area 2D Mo2C on in situ grown graphene, Adv. Mater. 29 (2017) 1700072.
[85] D. Wang, C. Zhou, A.S. Filatov, W. Cho, F. Lagunas, M. Wang, S. Vaikuntanathan, C. Liu, R.F. Klie, D.V. Talapin, Direct synthesis and chemical vapor deposition of 2D carbide and nitride MXenes, Science 379 (2023) 1242–1247.
[86] V. Thirumal, R. Yuvakkumar, P.S. Kumar, G. Ravi, S.P. Keerthana, D. Velauthapillai, Facile single-step synthesis of MXene@ CNTs hybrid nanocomposite by CVD method to remove hazardous pollutants, Chemosphere 286 (2022) 131733.
[87] M. Alhabeb, K. Maleski, B. Anasori, P. Lelyukh, L. Clark, S. Sin, Y. Gogotsi, Guidelines for synthesis and processing of two-dimensional titanium carbide (Ti3C2T x MXene), Chem. Mater. 29 (2017) 7633–7644.
[88] M. Naguib, M. Kurtoglu, V. Presser, J. Lu, J. Niu, M. Heon, L. Hultman, Y. Gogotsi, M.W. Barsoum, Two-dimensional nanocrystals produced by exfoliation of Ti3AlC2, in: MXenes, Jenny Stanford Publishing, 2011: pp. 15–29.
[89] K. Zhu, Y. Jin, F. Du, S. Gao, Z. Gao, X. Meng, G. Chen, Y. Wei, Y. Gao, Synthesis of Ti2CTx MXene as electrode materials for symmetric supercapacitor with capable volumetric capacitance, Journal of Energy, Chemistry 31 (2019) 11–18.
[90] B. Soundiraraju, B.K. George, Two-dimensional titanium nitride (Ti2N) MXene: synthesis, characterization, and potential application as surface-enhanced Raman scattering substrate, ACS Nano 11 (2017) 8892–8900.
[91] M. Naguib, O. Mashtalir, J. Carle, V. Presser, J. Lu, L. Hultman, Y. Gogotsi, M. W. Barsoum, Two-dimensional transition metal carbides, ACS Nano 6 (2012) 1322–1331.
[92] J. Zhou, X. Zha, F.Y. Chen, Q. Ye, P. Eklund, S. Du, Q. Huang, A two-dimensional zirconium carbide by selective etching of Al3C3 from nanolaminated Zr3Al3C5, Angew. Chem. Int. Ed. 55 (2016) 5008–5013.
[93] X. Zhang, W. Zhang, H. Zhao, Ultrasound-assisted fabrication of Ti3C2Tx MXene toward enhanced energy storage performance, Ultrason. Sonochem. 86 (2022) 106024.
[94] J. Halim, S. Kota, M.R. Lukatskaya, M. Naguib, M. Zhao, E.J. Moon, J. Pitock, J. Nanda, S.J. May, Y. Gogotsi, Synthesis and characterization of 2D molybdenum carbide (MXene), Adv. Funct. Mater. 26 (2016) 3118–3127.
[95] F. Liu, J. Zhou, S. Wang, B. Wang, C. Shen, L. Wang, Q. Hu, Q. Huang, A. Zhou, Preparation of high-purity V2C MXene and electrochemical properties as Li-ion batteries, J. Electrochem. Soc. 164 (2017) A709.
[96] P. Urbankowski, B. Anasori, T. Makaryan, D. Er, S. Kota, P.L. Walsh, M. Zhao, V. B. Shenoy, M.W. Barsoum, Y. Gogotsi, Synthesis of two-dimensional titanium nitride Ti 4 N 3 (MXene), Nanoscale 8 (2016) 11385–11391.
[97] F. Du, H. Tang, L. Pan, T. Zhang, H. Lu, J. Xiong, J. Yang, C.J. Zhang, Environmental friendly scalable production of colloidal 2D titanium carbonitride MXene with minimized nanosheets restacking for excellent cycle life lithium-ion batteries, Electrochim. Acta 235 (2017) 690–699.
[98] J. Halim, M.R. Lukatskaya, K.M. Cook, J. Lu, C.R. Smith, L.-Å. Näslund, S.J. May, L. Hultman, Y. Gogotsi, P. Eklund, Transparent conductive two-dimensional titanium carbide epitaxial thin films, Chem. Mater. 26 (2014) 2374–2381.
[99] J. Chen, W. Qin, K. Li, L. Feng, J. Chen, H. Qiao, M. Yang, Z. Tian, X. Li, C. Gu, A high-sensitivity, fast-response and high-stability humidity sensor of curly flake Ti 3 C 2 T x MXene prepared by electrolytic intercalation of NaOH solution, J. Mater. Chem. A 10 (2022) 22278–22288.
[100] M. Han, K. Maleski, C.E. Shuck, Y. Yang, J.T. Glazar, A.C. Foucher, K. Hantanasirisakul, A. Sarycheva, N.C. Frey, S.J. May, Tailoring electronic and optical properties of MXenes through forming solid solutions, J. Am. Chem. Soc. 142 (2020) 19110–19118.
[101] H. Jiang, L. Zheng, Z. Liu, X. Wang, Two-dimensional materials: From mechanical properties to flexible mechanical sensors, InfoMat 2 (2020) 1077–1094.
[102] J.-C. Lei, X. Zhang, Z. Zhou, Recent advances in MXene: Preparation, properties, and applications, Frontiers of Physics 10 (2015) 276–286.
[103] K.A.S. Usman, J. Zhang, C.J.O. Bacal, S. Qin, P. Mota-Santiago, P.A. Lynch, M. Naebe, L.C. Henderson, D. Hegh, J.M. Razal, Tension-induced toughening and conductivity enhancement in sequentially bridged MXene fibers, 2D Materials 9 (2022) 44003.
[104] J. Lv, X. Li, Z. An, Y. Wu, Z. Shi, G. Liu, Y. Lu, F. Zhang, J. Liu, X. Chen, Touch-activated information interaction system based on body-heat-powered flexible thermoelectric generator for food spoilage monitoring, Nano Energy 109418 (2024).
[105] M. Kotal, A.K. Bhowmick, Polymer nanocomposites from modified clays: Recent advances and challenges, Prog. Polym. Sci. 51 (2015) 127–187.
[106] O. Zabihi, M. Ahmadi, S. Nikafshar, K.C. Preyeswary, M. Naebe, A technical review on epoxy-clay nanocomposites: Structure, properties, and their applications in fiber reinforced composites, Compos. B Eng. 135 (2018) 1–24.
[107] L. Li, L. Maddalena, Y. Nishiyama, F. Carosio, Y. Ogawa, L.A. Berglund, Recyclable nanocomposites of well-dispersed 2D layered silicates in cellulose nanofibril (CNF) matrix, Carbohydr. Polym. 279 (2022) 119004.
[108] P. Kiliaris, C.D. Papaspyrides, Polymer/layered silicate (clay) nanocomposites: an overview of flame retardancy, Prog. Polym. Sci. 35 (2010) 902–958.
[109] H. Fischer, Polymer nanocomposites: from fundamental research to specific applications, Mater. Sci. Eng. C 23 (2003) 763–772.
[110] M. Tahriri, M. Del Monico, A. Moghanian, M.T. Yaraki, R. Torres, A. Yadegari, L. Tayebi, Graphene and its derivatives: Opportunities and challenges in dentistry, Mater. Sci. Eng. C 102 (2019) 171–185.
[111] S. Torres-Giner, Y. Echegoyen, R. Teruel-Juanes, J.D. Badia, A. Ribes-Greus, J. M. Lagaron, Electrospun poly (ethylene-co-vinyl alcohol)/graphene nanoplatelets composites of interest in intelligent food packaging applications, Nanomaterials 8 (2018) 745.
[112] M. Dervisevic, E. Dervisevic, M. Senel, E. Cevik, F.M. Abasiyanik, Novel amperometric xanthine biosensors based on REGO-NP (Pt, Pd, and Au) bionanocomposite film, Food Anal. Methods 10 (2017) 1252–1263.
[113] W. Liu, S. Kang, Q. Zhang, S. Chen, Q. Yang, B. Yan, Self-assembly fabrication of chitosan-tannic acid/MXene composite film with excellent antibacterial and antioxidant properties for fruit preservation, Food Chem. 410 (2023) 135405.
[114] D. Zhang, S. Yu, X. Wang, J. Huang, W. Pan, J. Zhang, B.E. Meteku, J. Zeng, UV illumination-enhanced ultrasensitive ammonia gas sensor based on (001) TiO2/MXene heterostructure for food spoilage detection, J. Hazard. Mater. 423 (2022) 127160.
[115] M. Gorji, A. Sadeghianmaryan, H. Rajabinejad, S. Nasherolahkam, X. Chen, Development of highly pH-sensitive hybrid membranes by simultaneous electrospinning of amphiphilic nanofibers reinforced with graphene oxide, Journal of Functional Biomaterials 10 (2019) 23.
[116] B.B. Maskey, K. Shrestha, J. Sun, H. Park, J. Park, S. Parajuli, S. Shrestha, Y. Jung, S. Ramasundaram, G.R. Koirala, Proving the robustness of a PEDOT: PSS-based thermistor via functionalized graphene oxide–poly (vinylidene fluoride) composite encapsulation for food logistics, RSC Adv. 10 (2020) 12407–12414.
[117] S. Jafarzadeh, M. Forough, V.J. Kouzegaran, M. Zargar, F. Garavand, M. Azizi-Lalabadi, M. Abdollahi, S.M. Jafari, Improving the functionality of biodegradable food packaging materials via porous nanomaterials, Compr. Rev. Food Sci. Food Saf. (2023).
[118] C. Chen, J. Xu, Y. Yao, SIW resonator humidity sensor based on layered black phosphorus, Electron. Lett 53 (2017) 249–251.
[119] R. Liu, Z. Cai, Q. Zhang, H. Yuan, G. Zhang, Colorimetric two-dimensional photonic crystal biosensors for label-free detection of hydrogen peroxide, Sens. Actuators, B 354 (2022) 131236.
[120] W. Shen, C. Wang, S. Zheng, B. Jiang, J. Li, Y. Pang, C. Wang, R. Hao, R. Xiao, Ultrasensitive multichannel immunochromatographic assay for rapid detection of foodborne bacteria based on two-dimensional film-like SERS labels, J. Hazard. Mater. 437 (2022) 129347.
[121] R. of R.C.A. as pH-S.P. in S.F.P. and S. Abedi-Firoozjah, S. Yousefi, M. Heydari, F. Seyedfatehi, S. Jafarzadeh, R. Mohammadi, M. Rouhi, F. Garavand, Application of

Red Cabbage Anthocyanins as pH-Sensitive Pigments in Smart Food Packaging and Sensors, Polymers (Basel) 14 (2022) 1629.
[122] N. Rabiee, M.R. Dokmeci, A. Zarrabi, P. Makvandi, M.R. Saeb, H. Karimi-Maleh, S. Jafarzadeh, C. Karaman, Y. Yamauchi, M.E. Warkiani, Green Biomaterials: fundamental principles, Green Biomaterials 1 (2023) 1–4.
[123] M.C. Christodoulou, J.C. Orellana Palacios, G. Hesami, S. Jafarzadeh, J. M. Lorenzo, R. Domínguez, A. Moreno, M. Hadidi, Spectrophotometric methods for measurement of antioxidant activity in food and pharmaceuticals, Antioxidants 11 (2022) 2213.
[124] Y. Zhao, J. Du, H. Zhou, S. Zhou, Y. Lv, Y. Cheng, Y. Tao, J. Lu, H. Wang, Biodegradable intelligent film for food preservation and real-time visual detection of food freshness, Food Hydrocoll. 129 (2022) 107665.
[125] S. Huang, H. Li, Y. Wang, X. Liu, H. Li, Z. Zhan, L. Jia, L. Chen, Monitoring of oxygen using colorimetric indicator based on graphene/TiO2 composite with first-order kinetics of methylene blue for modified atmosphere packaging, Packag. Technol. Sci. 31 (2018) 575–584.
[126] T. Le, V. Lakafosis, Z. Lin, C.P. Wong, M.M. Tentzeris, Inkjet-printed graphene-based wireless gas sensor modules, in: 2012 IEEE 62nd Electronic Components and Technology Conference, IEEE, 2012: pp. 1003–1008.
[127] A. Beniwal, P. Ganguly, A.K. Aliyana, G. Khandelwal, R. Dahiya, Screen-printed graphene-carbon ink based disposable humidity sensor with wireless communication, Sens. Actuators, B 374 (2023) 132731.
[128] Y. Jung, J. Min, J. Choi, J. Bang, S. Jeong, K.R. Pyun, J. Ahn, Y. Cho, S. Hong, S. Hong, Smart paper electronics by laser-induced graphene for biodegradable real-time food spoilage monitoring, Appl. Mater. Today 29 (2022) 101589.
[129] N.F.A. Kasim, W.F.W. Idris, A.H. Abdullah, K. Yusoh, Z. Ismail, The preparation of graphene ink from the exfoliation of graphite in pullulan, chitosan and alginate for strain-sensitive paper, Int. J. Biol. Macromol. 153 (2020) 1211–1219.
[130] F. Garavand, D. Khodaei, N. Mahmud, J. Islam, I. Khan, S. Jafarzadeh, R. Tahergorabi, I. Cacciotti, Recent progress in using zein nanoparticles-loaded nanocomposites for food packaging applications, Crit. Rev. Food Sci. Nutr. (2022) 1–21.
[131] S. Jafarzadeh, M. Forough, S. Amjadi, V. Javan Kouzegaran, H. Almasi, F. Garavand, M. Zargar, Plant protein-based nanocomposite films: A review on the used nanomaterials, characteristics, and food packaging applications, Crit. Rev. Food Sci. Nutr. (2022) 1–27.
[132] F. Garavand, M. Rouhi, S. Jafarzadeh, D. Khodaei, I. Cacciotti, M. Zargar, S. Hadi, Tuning the physicochemical, structural, and antimicrobial attributes of whey-based poly L-lactic acid (PLLA) films by chitosan nanoparticles, Front Nutr (n.d.) 793.
[133] M. Fathi, A. Babaei, H. Rostami, Development and characterization of locust bean gum-Viola anthocyanin-graphene oxide ternary nanocomposite as an efficient pH indicator for food packaging application, Food Packag. Shelf Life 34 (2022) 100934.
[134] T.-Y. Zhang, H. Wang, J. Tong, J. Zhang, X. Wang, Y. Zeng, High-efficiency ultraviolet shielding and high transparency of Ti3C2Tx MXene/poly (vinyl alcohol) nanocomposite films, Compos. Commun. 33 (2022) 101235.
[135] X. Wang, X. Li, L. Cui, Y. Liu, S. Fan, Improvement of gas barrier properties for biodegradable poly (butylene adipate-co-terephthalate) nanocomposites with MXene nanosheets via biaxial stretching, Polymers 14 (2022) 480.
[136] S. Tang, Z. Wu, X. Li, F. Xie, D. Ye, E. Ruiz-Hitzky, L. Wei, X. Wang, Nacre-inspired biodegradable nanocellulose/MXene/AgNPs films with high strength and superior gas barrier properties, Carbohydr. Polym. 299 (2023) 120204.
[137] S. Jafarzadeh, M. Forough, S. Amjadi, V. Javan Kouzegaran, H. Almasi, F. Garavand, M. Zargar, Plant protein-based nanocomposite films: A review on the used nanomaterials, characteristics, and food packaging applications, Crit. Rev. Food Sci. Nutr. 63 (2023) 9667–9693.
[138] F. Garavand, I. Cacciotti, N. Vahedikia, A. Rehman, Ö. Tarhan, S. Akbari-Alavijeh, R. Shaddel, A. Rashidinejad, M. Nejatian, S. Jafarzadeh, A comprehensive review on the nanocomposites loaded with chitosan nanoparticles for food packaging, Crit. Rev. Food Sci. Nutr. 62 (2022) 1383–1416.
[139] S.M. Eskandarabadi, M. Mahmoudian, K.R. Farah, A. Abdali, E. Nozad, M. Enayati, Active intelligent packaging film based on ethylene vinyl acetate nanocomposite containing extracted anthocyanin, rosemary extract and ZnO/Fe-MMT nanoparticles, Food Packag. Shelf Life 22 (2019) 100389.
[140] H. Moustafa, M. Morsy, M.A. Ateia, F.M. Abdel-Haleem, Ultrafast response humidity sensors based on polyvinyl chloride/graphene oxide nanocomposites for intelligent food packaging, Sens. Actuators, A 331 (2021) 112918.
[141] F. Garavand, S. Jafarzadeh, I. Cacciotti, N. Vahedikia, Z. Sarlak, Ö. Tarhan, S. Yousefi, M. Rouhi, R. Castro-Muñoz, S.M. Jafari, Different strategies to reinforce the milk protein-based packaging composites, Trends Food Sci. Technol. 123 (2022) 1–14.
[142] S. Jafarzadeh, A. Salehabadi, S.M. Jafari, 10 Metal nanoparticles as antimicrobial agents in food packaging, (2020).
[143] Z. Moslehi, A. Mohammadi Nafchi, M. Moslehi, S. Jafarzadeh, Aflatoxin, microbial contamination, sensory attributes, and morphological analysis of pistachio nut coated with methylcellulose, Food Sci. Nutr. 9 (2021) 2576–2584.
[144] W. Zhang, M. Azizi-Lalabadi, S. Jafarzadeh, S.M. Jafari, Starch-gelatin blend films: A promising approach for high-performance degradable food packaging, Carbohydr. Polym. 121266 (2023).
[145] A. Sadi, H. Ferfera-Harrar, Cross-linked CMC/Gelatin bio-nanocomposite films with organoclay, red cabbage anthocyanins and pistacia leaves extract as active intelligent food packaging: colorimetric pH indication, antimicrobial/antioxidant properties, and shrimp spoilage tests, Int. J. Biol. Macromol. 242 (2023) 124964.
[146] T.J. Gutiérrez, I.E. León, A.G. Ponce, V.A. Alvarez, Active and PH-sensitive nanopackaging based on polymeric anthocyanin/natural or organo-modified montmorillonite blends: characterization and assessment of cytotoxicity, Polymers 14 (2022) 4881.
[147] S. Jafarzadeh, A.K. Alias, F. Ariffin, S. Mahmud, A. Najafi, M. Ahmad, Fabrication and characterization of novel semolina-based antimicrobial films derived from the combination of ZnO nanorods and nanokaolin, J. Food Sci. Technol. 54 (2017), https://doi.org/10.1007/s13197-016-2441-3.
[148] S. Jafarzadeh, F. Ariffin, S. Mahmud, A.K. Alias, S.F. Hosseini, M. Ahmad, Improving the physical and protective functions of semolina films by embedding a blend nanofillers (ZnO-nr and nano-kaolin), Food Packag. Shelf Life 12 (2017), https://doi.org/10.1016/j.fpsl.2017.03.001.
[149] S. Jafarzadeh, A.K. Alias, F. Ariffin, S. Mahmud, A. Najafi, M. Ahmad, Fabrication and characterization of novel semolina-based antimicrobial films derived from the combination of ZnO nanorods and nanokaolin, J. Food Sci. Technol. 54 (2017) 105–113.
[150] S. Jafarzadeh, M. Hadidi, M. Forough, A.M. Nafchi, A. Mousavi Khaneghah, The control of fungi and mycotoxins by food active packaging: A review, Crit. Rev. Food Sci. Nutr. 63 (2023) 6393–6411.
[151] S. Bhatt, R. Pathak, V.D. Punetha, M. Punetha, Recent advances and mechanism of antimicrobial efficacy of graphene-based materials: a review, J. Mater. Sci. 58 (2023) 7839–7867.
[152] K.S. Prashanth, V. Revathi, Antimicrobial and antifungal studies of polymer nanocomposites with 2D nanomaterials, Mater. Today:. Proc. 49 (2022) 593–596.
[153] X. Santos, M. Álvarez, D. Videira-Quintela, A. Mediero, J. Rodríguez, F. Guillén, J. Pozuelo, O. Martín, Antibacterial capability of MXene (Ti3C2Tx) to produce PLA active contact surfaces for Food Packaging Applications, Membranes 12 (2022) 1146.
[154] C.D. Grande, J. Mangadlao, J. Fan, A. De Leon, J. Delgado-Ospina, J.G. Rojas, D.F. Rodrigues, R. Advincula, Chitosan cross-linked graphene oxide nanocomposite films with antimicrobial activity for application in food industry, in: Macromolecular Symposia, Wiley Online Library, 2017: p. 1600114.
[155] Y.A. Arfat, J. Ahmed, M. Ejaz, M. Mullah, Polylactide/graphene oxide nanosheets/clove essential oil composite films for potential food packaging applications, Int. J. Biol. Macromol. 107 (2018) 194–203.
[156] A. Jayakumar, S. Mathew, S. Radoor, J.T. Kim, J.-W. Rhim, S. Siengchin, Recent advances in two-dimensional nanomaterials: Properties, antimicrobial, and drug delivery application of nanocomposites, Mater. Today Chem. 30 (2023) 101492.
[157] F.J. Godínez-García, R. Guerrero-Rivera, J.A. Martínez-Rivera, E. Gamero-Inda, J. Ortiz-Medina, Advances in two-dimensional engineered nanomaterials applications for the agro–and food-industries, J. Sci. Food Agric. 103 (2023) 5201–5212.
[158] A. Bhat, S. Anwer, K.S. Bhat, M.I.H. Mohideen, K. Liao, A. Qurashi, Prospects challenges and stability of 2D MXenes for clean energy conversion and storage applications, npj 2D Mater. Appl. 5 (2021) 61.
[159] Z. Qazanfarzadeh, V. Kumaravel, Hydrophobisation approaches of protein-based bioplastics, Trends Food Sci. Technol. (2023).
[160] K.A. Mitura, P.K. Zarzycki, Biocompatibility and toxicity of allotropic forms of carbon in food packaging, Role of Materials Science in Food Bioengineering (2018) 73–107.
[161] G. Peng, B. Fadeel, Understanding the bidirectional interactions between two-dimensional materials, microorganisms, and the immune system, Adv. Drug Deliv. Rev. 188 (2022) 114422.
[162] R. Bayan, N. Karak, Polymer nanocomposites based on two-dimensional nanomaterials, in: Two-Dimensional Nanostructures for Biomedical Technology, Elsevier, 2020: pp. 249–279.